Pressure Swing Adsorption Reactors: Simulation of Three-Step One-Bed Process

Z. P. Lu and A. E. Rodrigues
Lab. of Separation and Reaction Engineering, School of Engineering, University of Porto, 4099 Porto Codex, Portugal

A three-step (feed, delay, and purge), one-column pressure swing adsorption reactor has been analyzed. An equilibrium model taking into account species mass balances, overall mass balance, momentum balance, reaction rate, and nonlinear multicomponent adsorption equilibrium isotherms was derived to describe the PSA reactor process. Numerical solution of model equations was obtained by using the method of orthogonal collocation on finite elements, and simulation results showed that 10–20% higher conversion than reaction equilibrium conversion in a fixed-bed reactor could be obtained from the PSA reactor for a reversible reaction $A \rightleftarrows B + C$, such as dehydrogenation of ethane to ethylene and hydrogen on cadmium-exchanged zeolites, where only product B was assumed to be adsorbed. When both reactant A and product B are adsorbed, 10% higher conversion over the reaction equilibrium limit was observed for pure reactant feed. The effects of system and operating parameters on the process performance of the PSA reactor have been studied, as well as the bed dynamics of the PSA reactor at the cyclic steady state.

Introduction

The advantages of coupling chemical reaction and separation by adsorption have been recognized for more than 30 years in the area of chromatography. The first works were started almost simultaneously by Magee (1963) and Roginskii et al. (1961). Recently, these topics are receiving more and more attention, as illustrated by a chapter on chromatographic reactors by Ganetsos and Barker (1993). Matsen et al. (1965) presented four conditions they felt were necessary for a chromatographic reactor to be efficient. First, the reaction must be reversible and the equilibrium rate should be small. Secondly, the separation of products should limit the reaction, that is, the reaction rate should be relatively high. Thirdly, at least two chromatographic separable products must be formed. Finally, reactants must not be separated in reactors. However, Wetherold et al. (1974) pointed out that it is not necessary that all these four conditions be met.

In gas chromatographic reactors, a reversible reaction $A \rightleftarrows B + nC$ is normally considered. Experimental examples can be found such as dehydrogenation of cyclohexane to benzene and hydrogen carried out on Pt/alumina supported catalysts ($n = 3$, Matsen et al., 1965; Schweich and Villermaux, 1982) and dehydrogenation of ethane to ethylene and hydrogen on *Cd* exchanged zeolites ($n = 1$, Antonucci et al., 1980). In these chromatographic reactors, the products *B* and *C* show different adsorption behavior on the adsorbents, alumina, and zeolites. *C* is hydrogen which is not adsorbed and then it is removed from the reactive zone, whereas it is separated from the adsorbable species *B* (benzene or ethylene). Finally, the reversible reaction equilibrium is shifted to the right side to a higher extent than that corresponding to a steady-state operation. Conversions higher than the reaction equilibrium limits for dehydrogenation of cyclohexane and ethane, respectively, were experimentally found in chromatographic reactors (Roginskii et al., 1961; Magee, 1963; Matsen et al., 1965; Schweich and Villermaux, 1982; Antonucci et al., 1978) and in a rotating annular gas chromatographic reactor (Carr, 1993).

However, preparative applications of chromatographic reactors are still at early stages (Sardin, et al., 1993; Carr, 1993; Coca et al., 1993). Only a few cyclic separating reactor schemes have been investigated: pulsed chromatographic reactors and simulated moving adsorptive reactors. Applications of these cyclic operating schemes can be found mainly in bioreaction and separations (Ganetsos et al., 1993; Hashimoto et al., 1993; van der Wielen et al., 1993). Much of the work in chromatographic reactors has been theoretically studied through mod-

Correspondence concerning this article should be addressed to A. E. Rodrigues.

eling (Schweich and Villermaux, 1982; Viswanathan and Aris, 1974; Petroulas et al., 1985; Loureiro et al., 1993; Sardin et al., 1993; Carta, 1991). Carr and co-workers (Carr, 1993; Fish and Carr, 1989; Petroulas et al., 1985) studied the catalytic hydrogenation of mesitylene (MES) on Pt/Al_2O_3 by using a countercurrent moving-bed chromatographic reactor (CMCR). Their mathematical analysis was supported by experimental results; much higher reaction conversion than the reaction equilibrium and almost pure reaction product could be obtained by choosing the operating conditions carefully.

Recently, a scheme of rapid-cycle single-bed pressure swing adsorption (PSA) combined with periodic reactor operation in which feed components are simultaneously reacted and separated has been described and studied experimentally by Vaporciyan and Kadlec (1987, 1989). Their cyclic operation consists of three steps: feed, delay, and exhaust. They claimed that this kind of periodic separating reactors can also be applied to multistep, multibed, or rotational forms of PSA. The CO oxidation over a packed bed with layers of supported platinum catalyst and 5 Å molecular sieve adsorbents was experimentally studied, and the perturbed equilibrium model and the reaction rate limited model for irreversible and reversible reactions were presented. Three-step and four-step PSA reactor processes were also studied theoretically by Chatsiriwech et al. (1993) for a reversible reaction without changes in number of moles. They found that the inclusion of the purge step in the cyclic operation leads to a significant increase in conversion since a relative short exhaust step time was used in their simulations.

The cyclic scheme of PSA reactor processes is a good preparative application of the gas chromatographic reactor since it provides high catalyst productivity and better conversion than the reaction equilibrium limit. In our last work (Lu et al., 1993a), an operation scheme of the three-step one-column PSA reactor process with pure reactant feed was studied. General results showed that conversion higher than that corresponding to the reaction equilibrium limit can be obtained.

The objectives of this article will be focused on the process performance and dynamics of the one-column PSA reactor process, for cases of pure and impure reactant feed and introduction of product purge in the cyclic operation.

Process Description

The PSA reactor process to be modeled in this article is similar to that used in rapid PSA separation process (Lu et al., 1993b), a three-step one-column process, shown in Figure 1. There are three species, A, B, and C if the feed is pure reactant A, or four species A, B, C, and I if the feed is a mixture of A and I (I is assumed to be nonadsorbable), in the PSA reactor operation considered in this article.

The chemical reaction described in Eq. 1, such as dehydrogenation of ethane (A) to ethylene (B) and hydrogen (C), is considered in this article.

$$A \underset{k_2}{\overset{k_1}{\rightleftarrows}} B + C \tag{1}$$

The reaction rate is:

$$r_A = k_1 c_A - k_2 c_B c_C = k_1 (c_A - K_e c_B c_C) \tag{1a}$$

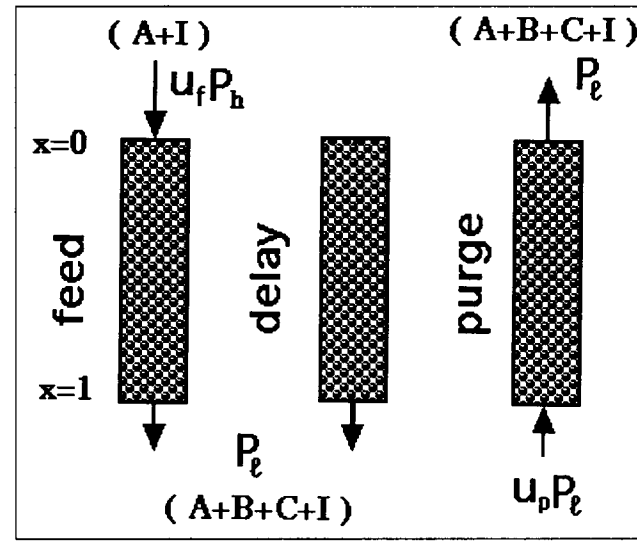

Figure 1. Operating scheme of the three-step, one-bed PSA reactor.

where $K_e = k_2/k_1$. A and B are adsorbed on the catalyst/adsorbent supports and they follow the multicomponent Langmuir isotherm which gives the same results as those calculated from the IAS (ideal adsorbed solution) theory when the adsorption capacity is identical for all species (Frey and Rodrigues, 1993):

$$q_i = \frac{q_m b_i c_i}{1 + \Sigma b_i c_i}; \quad i = A, B \tag{2}$$

Usually, B is more adsorbed than A (Schweich and Villermaux, 1978, 1982; Antonucci et al., 1978), and C is nonadsorbable. If A is also nonadsorbable, that is, $b_A = 0$, Eq. 2 reduces to single component Langmuir isotherm. It must be pointed out that the catalyst/adsorbent referred to in this article is active material supported on adsorbent, that is, the catalyst/adsorbent has the same adsorption behavior as the adsorbent; in previous work (Vaporciyan and Kadlec, 1987, 1989) adsorbent and catalyst are different particles. Pure reactant ethane or a mixture of ethane and inert I is used to feed the PSA reactor process. Low pressure, that is, atmospheric pressure, is favorable to the forward reaction because the catalytic dehydrogenation is a reaction with increase in the number of moles, so that the production and blowdown ends of the reactor are set at the low pressure. The following operating scheme of the three-step, one-column, PSA reactor process is considered (Figure 1):

Step 1 (*Feed*). Feeding the reactor bed at the feed side with feed stream and opening the bed at the other side at the low pressure. A pressure gradient inside the bed is created due to the use of very small particles and very large feed rate.

Step 2 (*Delay*). Closing the feed side of the bed and keeping the other side of the bed open for a while.

Step 3 (*Purge*). Opening the feed end of the bed at the low pressure and introducing a product stream, that is, obtained in step 1 and step 2, at the other end of the bed to purge the reactor. Therefore, species remaining inside the bed will be pushed out of the bed. Then the process is cycled. The reactant A is consumed to give B and C continuously, and

enriched B and C will be obtained one at each side of the reactor bed. The proposed operating scheme considers a purge step instead of an exhaust step (Vaporciyan and Kadlec, 1987, 1989).

Mathematical Model

A simple mathematical model, the local equilibrium model for adsorption in which the finite reaction rate is taken into account (Lu et al., 1993a), is used to simulate the processes described above.

The main assumptions for the mathematical model are:

(1) Temperature changes are assumed to be negligible, that is, isothermal operation.
(2) Mass-transfer resistances are assumed to be negligible.
(3) The flow pattern can be described by the axial dispersed plug flow.
(4) The superficial fluid velocity in the bed follows Ergun's relation locally.
(5) The dead volumes at both side of the reactor are assumed to be negligible (Lu et al., 1993b).

The model developed by Vaporciyan and Kadlec (1987) considers linear adsorption equilibrium isotherms and Darcy's law for flow in the bed.

Introducing the dimensionless variables:

$$x=z/L,\ f=c/c_0=P/P_0,\ \theta=t/\tau_0,\ u^*=u/u_0$$

where c_o and P_o are the reference total concentration and pressure, u_o is the reference superficial velocity, and $\tau_o = \epsilon L/u_o$ is the reference space time. Model equations are:

Mass Balance for the Species i $(i=A, B, C)$.

$$\frac{\partial}{\partial x}\left(\frac{u^* f}{Pe}\frac{\partial y_i}{\partial x}\right)-\frac{\partial(u^* f y_i)}{\partial x}+r_i=\frac{\epsilon_t}{\epsilon}\left[\frac{\partial(f y_i)}{\partial\theta}+\epsilon_r\frac{\partial(q_i/c_o)}{\partial\theta}\right] \quad (3)$$

where the reaction rate is:

$$-r_A=r_B=r_C=Daf(y_A-K_T f y_B y_C) \quad (3a)$$

and

$$\frac{\partial(q_C/c_o)}{\partial\theta}=0 \quad (3b)$$

since C is nonadsorbable.

Overall Mass Balance.

$$-\frac{\partial(u^* f)}{\partial x}+Daf(y_A-K_T f y_B y_C)=\frac{\epsilon_t}{\epsilon}\left\{\frac{\partial f}{\partial\theta}+\epsilon_r\left[\frac{\partial(q_A/c_o)}{\partial\theta}+\frac{\partial(q_B/c_o)}{\partial\theta}\right]\right\} \quad (4)$$

where $\epsilon_r=[(1-\epsilon)(1-\epsilon_p)]/\epsilon_t$ and $\epsilon_t=\epsilon+(1-\epsilon)\epsilon_p$. The concentrations of species $i=A, B$ in the adsorbed phase are given by the multicomponent Langmuir isotherm, Eq. 2.

Two different initial conditions were used in the simulations; one considers that the reactor was initially saturated by the nonadsorbable species C or I; in the other the process starts with the bed saturated with a reaction equilibrated mixture of A, B, C, and I; mathematically:

Initial conditions are:

$$\theta=0,\quad f=f_i,\quad y_i=0\ (i=A, B),\quad y_C=1 \text{ and } y_C=0 \text{ if there is } D \quad (5)$$

or

$$\theta=0,\quad f=f_i,\quad y_A=\frac{y_{fA}-y_o}{1+y_o},\quad y_i=\frac{y_o}{1+y_o}\ (i=B, C) \quad (6)$$

where $y_o=y_{fA}X_A$ and y_{fA} is the feed mole fraction.

Boundary conditions for a given cycle considering time zero at the beginning of each step are (for the one-column case, Figure 1):

(*i*) *Feed (Step 1)* $(0\le\theta\le\theta_f)$.

$$x=0,\quad u^* f=u_f^* f_h,\quad -\frac{1}{Pe}\frac{\partial y_A}{\partial x}+y_A=1,\quad -\frac{1}{Pe}\frac{\partial y_i}{\partial x}+y_i=0\ (i=B, C) \quad (7)$$

$$x=1,\quad f=f_i,\quad \frac{\partial y_i}{\partial x}=0\ (i=A, B, C) \quad (8)$$

(*ii*) *Delay (Step 2)* $(0\le\theta\le\theta_d)$.

$$x=0,\quad \frac{\partial f}{\partial x}=0,\quad \frac{\partial y_i}{\partial x}=0\ (i=A, B, C) \quad (9)$$

$$x=1,\quad f=f_i,\quad \frac{\partial y_i}{\partial x}=0\ (i=A, B, C) \quad (10)$$

(*iii*) *Purge (Step 3)* $(0\le\theta\le\theta_p)$.

$$x=0,\quad f=f_i,\quad \frac{\partial y_i}{\partial x}=0\ (i=A, B, C) \quad (11)$$

$$x=1,\quad u^* f=-u_p^* f_i,\quad -\frac{1}{Pe}\frac{\partial y_i}{\partial x}+y_i=\bar{y}_{fi}\ (i=A, B, C) \quad (12b)$$

where $\bar{y}_{fi}$ is the average mole fraction of species i obtained at $x=1$ in the feed and delay steps.

The dimensionless cycle time $\theta_t=\theta_f+\theta_d+\theta_p$, where θ_t, θ_f, θ_d, and θ_p are the dimensionless total, feed, production, and blowdown times, respectively.

Momentum equation:

$$-\frac{\partial f}{\partial x}=b_3u^*+b_4 f(u^*)^2 \quad (13)$$

$$b_3=\frac{150\mu(1-\epsilon)^2L}{d_p^2\epsilon^3P_o}u_0;\quad b_4=\frac{1.75\rho_0(1-\epsilon)L}{P_o d_p\epsilon^3}u_o^2 \quad (13a)$$

Model parameters are

Axial Peclet number:

$$\frac{1}{Pe}=\frac{\epsilon D_{ax}}{Lu}=\frac{b_1}{u^* f}+b_2;\quad b_1=\frac{\epsilon\gamma_1 D_{mo}}{Lu_o};\quad b_2=\frac{\epsilon\gamma_2 d_p}{L} \tag{14}$$

Multicomponent equilibrium adsorption isotherm parameters:

$$q_m;\quad b_i'=b_i c_o\ (i=A,\ B) \tag{15}$$

Reaction equilibrium constant:

$$K_T=K_e c_o \tag{16}$$

Reaction Damköhler number:

$$Da=\frac{1-\epsilon}{\epsilon}\,k_1\tau_0 \tag{17}$$

Process Performance

The process performance of a PSA reactor at the cyclic steady state can be described by the following parameters.

Conversion of the reactant A:

$$X_A=\frac{N_B}{N_A+N_B} \tag{18}$$

where N_A, N_B are the dimensionless output fluxes of species A and B in a cycle at the cyclic steady state normalized by the reference flux $u_o c_o$, that is:

$$N_i=\frac{1}{\theta_t}\left[\int_0^{\theta_f} u^* f y_i(x=1)d\theta+\int_0^{\theta_d} u^* f y_i(x=1)d\theta+\int_0^{\theta_p} u^* f y_i(x=0)d\theta\right]\ (i=A,\ B,\ C) \tag{19}$$

Productivity of the catalyst expressed in mol/m^3·s is:

$$N_{\text{prod}}=c_o u_o N_B/L \tag{20}$$

where L is length of the catalyst/adsorbent layer.

Separation factor:

$$\alpha_{BA}=\frac{\bar{y}_{pB}\bar{y}_{fA}}{\bar{y}_{fB}\bar{y}_{pA}};\quad \alpha_{BC}=\frac{\bar{y}_{pB}\bar{y}_{fC}}{\bar{y}_{fB}\bar{y}_{pC}} \tag{21}$$

where $\bar{y}_{pi}$ and $\bar{y}_{fi}$ are the average mole fraction of components i ($i=A,\ B,\ C$) in streams obtained at $x=0$ and $x=1$, respectively.

Production ratio:

$$R_p=\frac{N_p}{N_t} \tag{22}$$

where N_p and N_t are the dimensionless output flux at the feed end ($x=0$) of the bed and total output flux in a cycle at the cyclic steady state, respectively.

For the fixed-bed reactor operation at the steady state, the model equations are the same as Eqs. 3, 4, 7, and 8. The righthand sides of Eqs. 3 and 4 are equal to zero.

Simulation Results and Discussion

Model equations were solved by using the PDECOL (Madsen and Sincovec, 1979) package which is based on the method of orthogonal collocation in finite elements. 25 elements were used normally in the calculations, then 100–120 s are needed for numerically simulating a cycle of the PSA reactor in an IBM RISC/6000 computer. In order to simulate the transitions of the boundary conditions from step to step in a cycle, an exponential time function was employed (Lu et al., 1993b). For the gas-phase dehydrogenation of ethane to ethylene and hydrogen on a cadmium-exchanged zeolite catalyst/adsorbent in a reactor, the values used in the numerical simulations taken from the works of Antonucci et al. (1978) and Schweich and Villermaux et al. (1982) are listed in Table 1.

Fixed-bed reactor operation at steady state

Before studying the PSA reactor, we first review the fixed-

Table 1. Values Used in the Simulations

Reactor Column	Parameters
	Bed length $L=100$ cm
Operating temperature $T=723$ K	Bed diameter $D=2.5$ cm
Production (low) pressure $P_l=1$ bar	Particle average diameter $d_p=0.02$ cm
Reference Conditions	Interparticle porosity $\epsilon=0.4$
$P_o=1$ bar	Intraparticle porosity $\epsilon_p=0.5$
$T_o=723$ K	*Rate Constant of the Forward Reaction*
$c_o=1.68\times10^{-2}$ mol/L	$k_1=1,\ 5,\ 10,\ 20,\ 50,\ 100\ s^{-1}$
$u_o=43.84$ cm/s	*Reaction Equilibrium Constant*
$\tau_o=0.913$ s	$K_e=1.48\times10^3$ (mol/L)$^{-1}$
Operating Conditions	*Adsorption Isotherm Parameters*
$u_f^* f_h=4.5$–27	$q_m=0.25,\ 0.5,\ 1.0$ mol/L
$u_p^* f_l=0.667$–3	$b_A=0,\ 10,\ 20$ L/mol; $b_B=50$ L/mol
$\theta_t=9$–15	*At the Reference Conditions*:
$y_{fA}=1.0,\ 0.5,\ 0.2$	Molecular diffusivity $D_{mo}=1.7$ cm^2/s
$R_p=0.5$–1.0	Fluid density $\rho_o=0.378\times10^{-3}$ g/cm^3
	Fluid viscosity $\mu=1.3\times10^{-4}$ g/cm·s
	Constants $\gamma_1=20$, $\gamma_2=0.5$

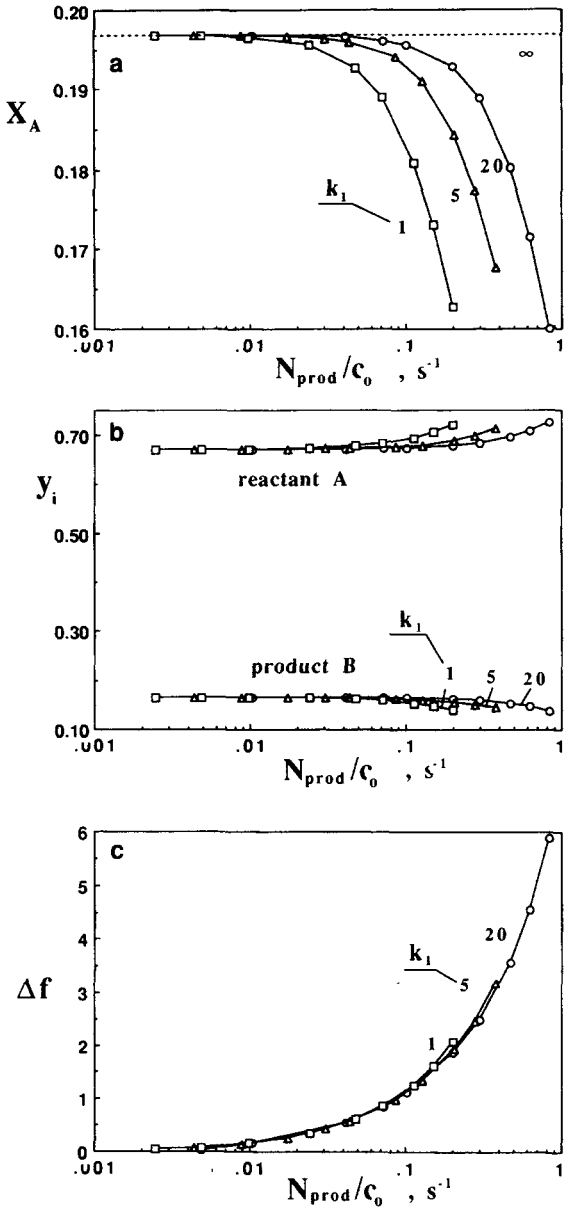

Figure 2. Numerical simulation results from the fixed-bed reactor operated at steady state for different kinetic constants $k_1 = 1, 5, 20\ s^{-1}$ for pure reactant feed $y_{fA} = 1$.

(a) Conversion of the reactant X_a as a function of the productivity of the catalyst N_{prod}/c_o; (b) mole fractions of species A and B at the bed outlet vs. N_{prod}/c_o; (c) dimensionless pressure drop across the bed vs. N_{prod}/c_o.

bed reactor operation at the steady state. Dehydrogenation reactions are usually very fast and reaction equilibrium constants are low. The number of moles increases with the extent of reaction so that the conversion at equilibrium increases when the operating total pressure decreases. In this study, the outlet of the reactor is set at the atmospheric pressure so the maximum conversion for pure reactant A feed is 0.1968 for the reaction equilibrium constant value given in Table 1. The steady-state conversion of the reactant A at the bed outlet, X_A, as a function of the productivity of the catalyst, N_{prod}/c_o, for different reaction kinetic constants k_1 is shown in Figure 2a. It can be seen that, at low catalyst productivity, the conversion corresponds to the equilibrium value. The conversion decreases when the catalyst productivity increases, that is, the fixed-bed reactor operation changes from an equilibrium controlled process to a kinetically controlled process. The higher is k_1 and the latter is the transition between these regimes. Figure 2b shows the mole fractions of A (reactant) and B (product) at the outlet of the reactor as a function of the catalyst productivity with k_1 as a parameter. Again a transition between equilibrium and kinetically controlled regimes is found, and the mole fractions of A and B change in opposite directions in the kinetic controlled regime. Finally, the pressure drop across the reactor, Δf ($\Delta f = \Delta P/P_o$), as a function of the catalyst productivity is shown in Figure 2c. Large pressure gradients inside the fixed-bed reactor were found for high catalyst productivity, and in these cases the fluid velocity inside the bed increases significantly from the inlet to the outlet of the reactor.

When the feed is a mixture of the reactant A and inert I, higher conversion of the reactant A is obtained which increases when the mole fraction of the reactant in the feed decreases. This is so since the effect of pressure on the reaction equilibrium decreases when more inert is present. When $y_{fA} = 0.2$ in the feed, the conversion, mole fractions of A and B, and the pressure drop across the reactor as functions of the productivity of the catalyst are shown in Figures 3a, 3b, and 3c, respectively. Now, the maximum conversion is 0.3694. Other behaviors are very similar to those we discussed above for pure reactant feed.

These results are the basis for assessing the performance of the new operating scheme for the PSA reactor process.

PSA reactors

Pressure swing adsorption (PSA) is a gas separation process which operates by shifting the partial pressure of the species to be separated due to their different adsorption behavior on the adsorbent. This PSA process, patented first by Skarstrom (1960), consists of four steps in a cycle; since then a wide variety of PSA processes have been established (Yang, 1987). Some rather complicated multistep cycles are currently used involving many beds and some rather simple cycles with less than four steps have also had considerable commercial interest.

Before simulation of the process is made, we should have a general understanding of the dehydrogenation catalytic reaction $A \rightleftarrows B + C$ in the PSA reactors. Various effects on the process performance of the PSA reactor process for a given reaction in isothermal operation mainly come from two groups of parameters: *system parameters*, that is, physical parameters, such as adsorption equilibrium, reaction kinetics, and feed compositions; *operating parameters*, such as feed and purge rates, step times, and the ratio between the feed and purge amounts. In this process, the reaction proceeds with increase in the number of moles, so low pressure is favorable to reactant conversion. However, low pressure decreases the used adsorption capacity of the adsorbent; therefore, less separation of the products B and C which is unfavorable to the reaction conversion. When the effect of the pressure on the reaction equilibrium dominates the process for some reactions with large increase in mole number, although the performance of the PSA reactor is better than that from the fixed-bed operation at some extreme operating conditions, it is unlikely to be suitable for preparative scale operation. For this reason the open side of the reactor in a cycle in this work is kept at atmospheric

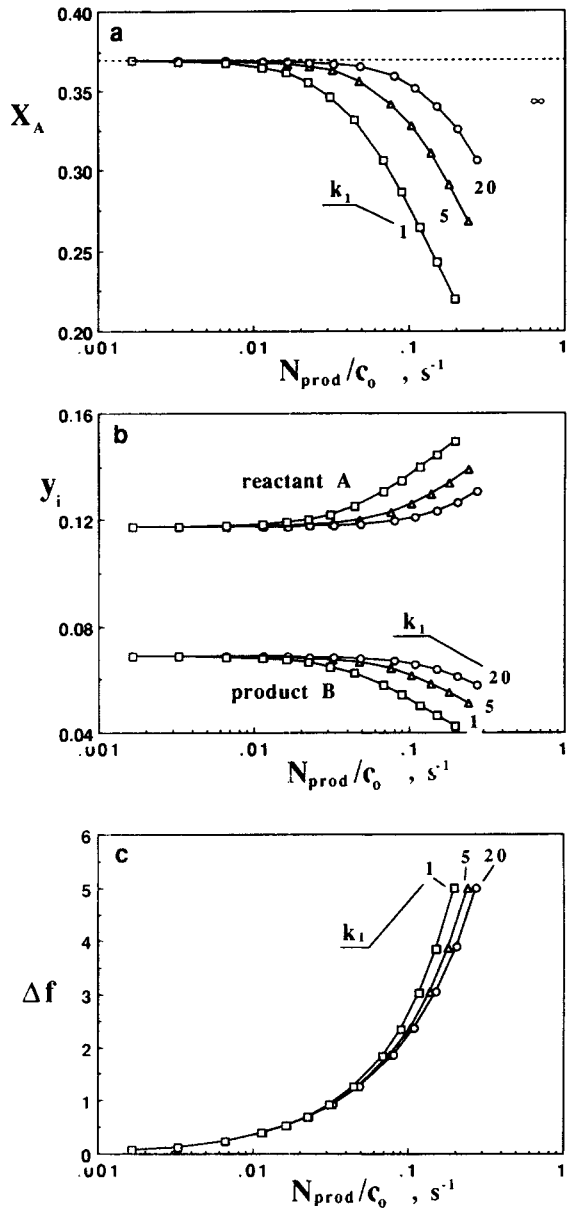

Figure 3. Numerical simulation results from the fixed-bed reactor operated at steady state for different kinetic constants $k_1 = 1, 5, 20\ s^{-1}$ for impure reactant feed $y_{fA} = 0.2$.

(a) Conversion of the reactant X_a as a function of the productivity of the catalyst N_{prod}/c_o; (b) mole fractions of species A and B at the bed outlet vs. N_{prod}/c_o; (c) dimensionless pressure drop across the bed vs. N_{prod}/c_o.

pressure, that is, $P_\ell = 1$ bar. In general, high feed and purge rates lead to high-pressure gradients locally and to low conversion. Low feed and purge rates mean low productivity of the catalyst/adsorbent which must be comparable with that of the fixed-bed reactor operation. The suitable feed and purge rates should be chosen from a trade-off between conversion and productivity. Usually, the higher the reaction kinetic rate, the higher is the conversion, that is, better process performance; the adsorption capacity of the adsorbent and the competitive adsorption coefficients of the adsorbable species are also important factors on the process performance. The simulations were carried out to understand how the performance of the PSA reactor process is influenced by: the nature of the adsorption equilibrium isotherm, $q_m = 0.25$, 0.5, 1.0 mol/L, $b_A = 0$, 10, 20 L/mol, and $b_B = 50$ L/mol; reaction kinetics, $k_1 = 5$, 10, 20, 50, 100 s^{-1}; feed compositions $y_{fA} = 1$, 0.5, 0.2; feed rates, $u_f^* f_h = 4.5$–27; and the ratios of feed and purge amounts resulting in $R_p = 0.5$–1.0. Next, we separate our discussions into two main groups: (I) only the product B is adsorbed, that is, $b_A = 0$, and (II) both reactant A and product B are adsorbed.

Only product B is adsorbed ($b_A = 0$)

Process Performance of the PSA Reactors. When the physical parameters are fixed, the selection of the operating parameters directly affects the process performance. For a given feed (purge) amount $u_f^* f_h \theta_f (u_p^* f_\ell \theta_p)$, there is a combination of using high feed (purge) rate, $u_f^* f_h (u_p^* f_\ell)$, and short feed (purge) time, $\theta_f (\theta_p)$, or low feed rate and long feed time. In simulations, it was found that the feed and purge rates do not significantly affect the conversion; however, the productivity of the catalyst/adsorbent directly depends on the purge rate which determines purge time for a given purge amount, since the purge time dominates the cycle time. Furthermore, it is necessary to use a relative long delay time to improve the conversion. In the simulations reported here, the operating parameters were unless noted: feed rate $u_f^* f_h = 9$, and feed time $\theta_f = 1$, that is, feed amount is fixed; purge rate $u_p^* f_\ell = 1$, and purge time θ_p varies from 5 to 11 which leads to a production ratio R_p from 0.5 to 1.0; and delay time $\theta_d = 2$. The reference parameters were: $u_o = 43.8$ cm/s, $\tau_o = 0.913$ s, $P_o = 1$ bar.

(*a*) *Effect of the Adsorption Capacity q_m and Feed Rate $u_f^* f_h$.* When the reactant A is nonadsorbable, the multicomponent extended Langmuir isotherm reduces to the single component Langmuir isotherm, and $b_B = 50$ mol/L was used throughout this work. If the feed stream is pure reactant A, there are three species A, B, and C in the system. In the feed and delay steps, reactant A continues to be converted to products B (adsorbable) and C; more B is retained inside the bed due to high pressure created by the high feed rate, and more C moves out of the bed from the open end. In the purge step, B is purged out of the bed at the feed end by the product obtained in the two steps above. The enhanced conversion X_A/X_o ($X_o = 0.1968$) over the reaction equilibrium limit and the separation factor α_{BA} (the selectivity of species B and A between the production streams obtained at $x = 1$ and at $x = 0$) as a function of the production ratio R_p for different adsorption capacities q_m ($q_m = 0.25$, 0.5, 1 mol/L) are shown in Figures 4a and 4b, respectively (full lines), where the feed stream composition is $y_{fA} = 1.0$ in the feed step and the kinetic constant is $k_1 = 20\ s^{-1}$. The conversion always increases with the production ratio for lower adsorption capacities $q_m = 0.25$ and 0.5 mol/L; for higher adsorption capacity $q_m = 1.0$ mol/L it goes through a maximum value. The separation factor seems to pass through a maximum value for the all three values of the adsorption capacities and its corresponding values of the production ratio increases with the adsorption capacity. In general, higher adsorption capacity results in better process performance, that is, higher conversion and higher separation factor. Higher production R_p means higher purge amount used in a

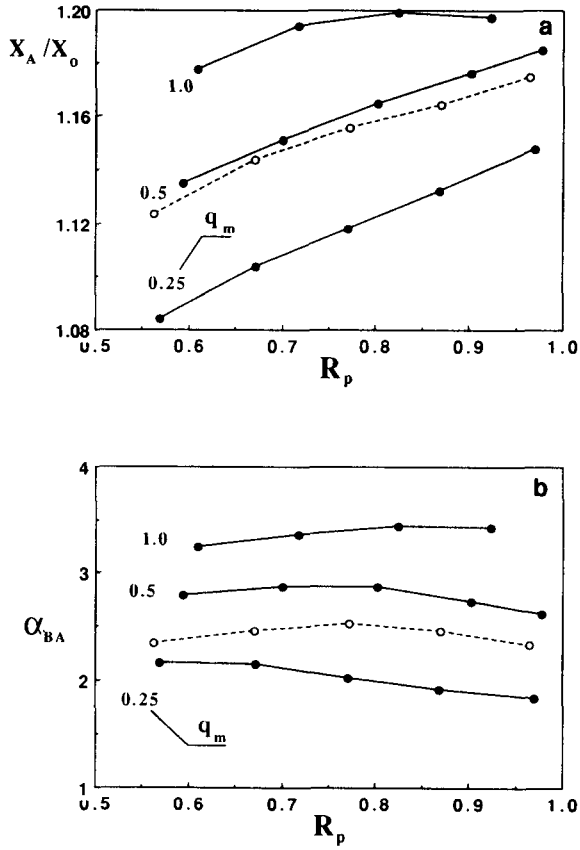

Figure 4. Process performance of the PSA reactor for pure reactant feed: $y_{fA}=1.0$, $b_A=0$, $b_B=50$ L/mol, $k_1=20$ s^{-1}, $q_m=0.25$, 0.5, 1.0 mol/L, $u_h^* f_h=9$, and $\theta_f=1$ for full lines and $u_h^* f_h=4.5$ and $\theta_f=2$ for dashed lines.

(a) Enhanced conversion of the reactant A, X_A/X_o vs. the production ratio R_p for different adsorption capacities q_m; (b) separation factor α_{BA} vs. R_p for different q_m.

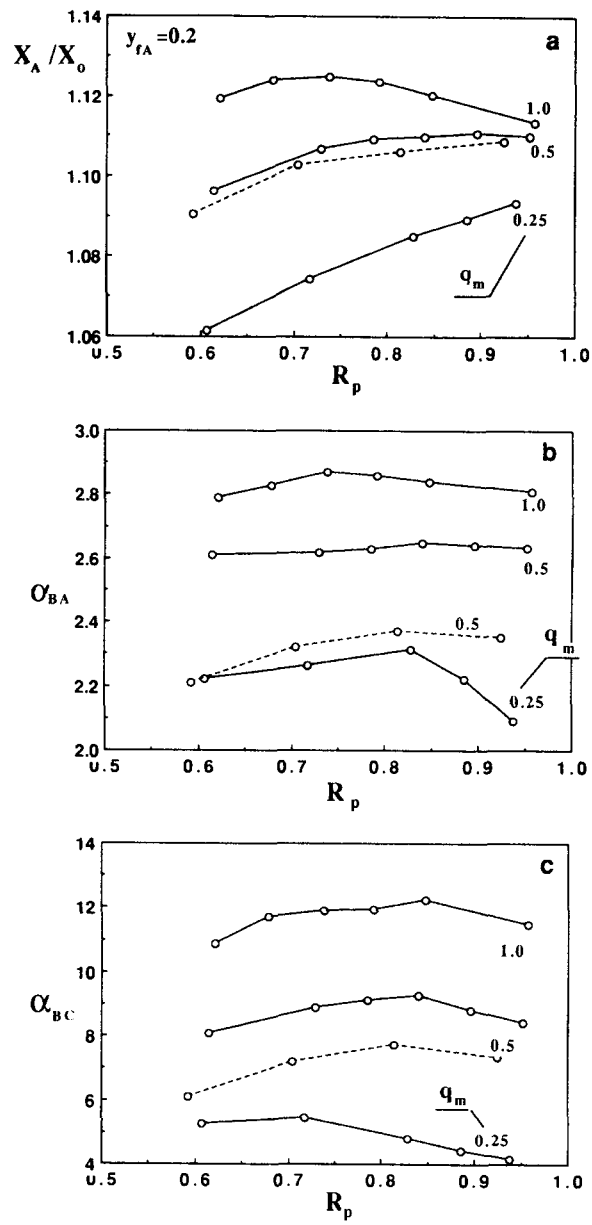

Figure 5. Process performance of the PSA reactor for impure reactant feed: $y_{fA}=0.2$, $b_A=0$, $b_B=50$ L/mol, $k_1=20$ s^{-1}, $q_m=0.25$, 0.5, 1.0 mol/L, $u_h^* f_h=9$, and $\theta_f=1$ for full lines and $u_h^* f_h=4.5$ and $\theta_f=2$ for dashed lines.

(a) Enhanced conversion of the reactant A, X_A/X_o vs. the production ratio R_p for different adsorption capacities q_m; (b) separation factor α_{BA} vs. R_p for different q_m; (c) separation factor α_{BA} vs. R_p for different q_m.

cycle for a given feed amount, that is, for a given productivity of the catalyst/adsorbent.

If the feed stream is a mixture of the reactant A and inert I, there are four species A, B, C, and D in the system. The enhanced conversion X_A/X_o ($X_o=0.3694$) and the separation factors α_{BA} and α_{BC} (the selectivity of species B and C between the production streams at $x=1$ and at $x=0$) as a function of the production ratio R_p for different adsorption capacities q_m ($q_m=0.25$, 0.5, 1 mol/L) are shown in Figure 5a, 5b, and 5c, respectively (full lines), where the feed stream composition is $y_{fA}=0.2$ in the feed step and the kinetic constant is $k_1=20$ s^{-1}. The general behavior of the process performance for impure reactant feed is very similar to that for pure reactant feed. Much better separation was found between species B and C (much higher α_{BC}) than between species B and A. The effect of the adsorption capacity on the separation factor α_{BA} is more obvious for pure reactant feed than for impure reactant feed by comparing Figure 4b and 5b; and the separation factors increase with the adsorption capacity. Larger increase of the conversion was observed from $q_m=0.25$ to 0.5 mol/L than from 0.5 to 1.0 mol/L in pure reactant feed and impure reactant feed; this is more obvious in the latter case, as shown in Figures 4a and 5a. However, the use of adsorbent/catalyst with higher adsorption capacity leads to higher conversion at relative lower production ratio R_p, that is, less energy consumption.

The effect of the feed rate was studied by using $u_f^* f_h=4.5$ and $\theta_f=2$ so the feed amount is kept the same as for $u_f^* f_h=9$ and $\theta_f=1$. The simulation results are shown in Figures 4 and 5 in dashed lines. Lower feed rate leads to lower pressure gradients locally, that is, lower pressure at the feed side of the reactor, and less used adsorption capacity for adsorbable spe-

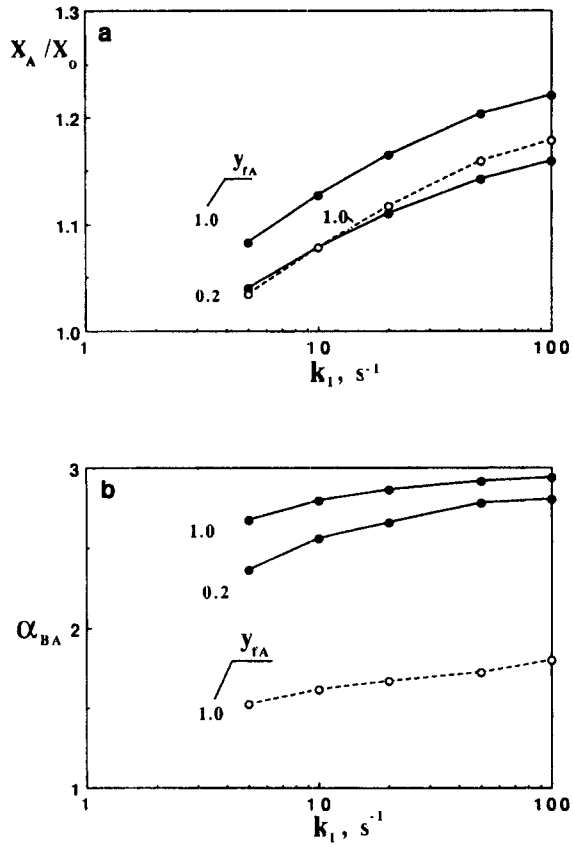

Figure 6. Enhanced conversion X_A/X_o (a) and separation factor α_{BA} as a function of the reaction kinetic constant k_1 for pure feed and impure feed for the case where only the product B is adsorbable $b_A = 0$ (full lines) and both reactant A and product B are adsorbable $b_A = 20$ L/mol (dashed lines).

cies B which results in lower separation factors and lower conversions. However, the maximum pressure drop across the bed in the cycle largely decreases from 4.41 to 2.84 bar when the feed rate $u_f^* f_h$ decreases from 9 to 4.5. It is expected that the better process performance, that is, a higher conversion and a higher separation factor can be obtained by using a lower purge rate; however, it will lead to a lower productivity of the catalyst-adsorbent particles.

(*b*) *Effect of Reaction Kinetic Constant k_1 and Feed Composition of the Reactant y_{fA}.* The enhanced reaction conversion X_A/X_o and the separation factor α_{BA} as a function of the reaction kinetic constant k_1 are shown in Figures 6a and 6b in full lines, respectively, where the simulation values used were: $q_m = 0.5$ mol/L, $R_p = 0.81$ for $y_{fA} = 1.0$, and $R_p = 0.84$ for $y_{fA} = 0.2$. For small kinetic constant k_1, the PSA reactor process is in the kinetic controlled regime; then the conversion and separation factor largely increase with k_1. For fast reactions, that is, high k_1, the process tends to fall into the reaction equilibrium controlled limit and the process performance parameters seem to reach their plateau values. This behavior is very similar to that found in the fixed-bed reactor operation at steady state as shown in Figures 2 and 3.

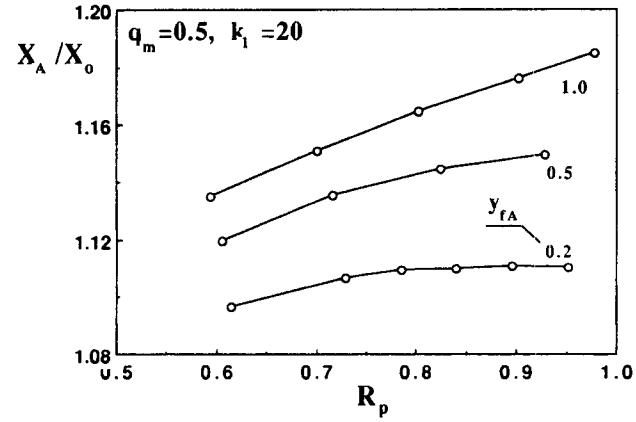

Figure 7. Enhanced conversion X_A/X_o as a function of the production ratio R_p for different feed compositions $y_{fA} = 0.2$, 0.5, 1.0 in the case where only the product B is adsorbable.

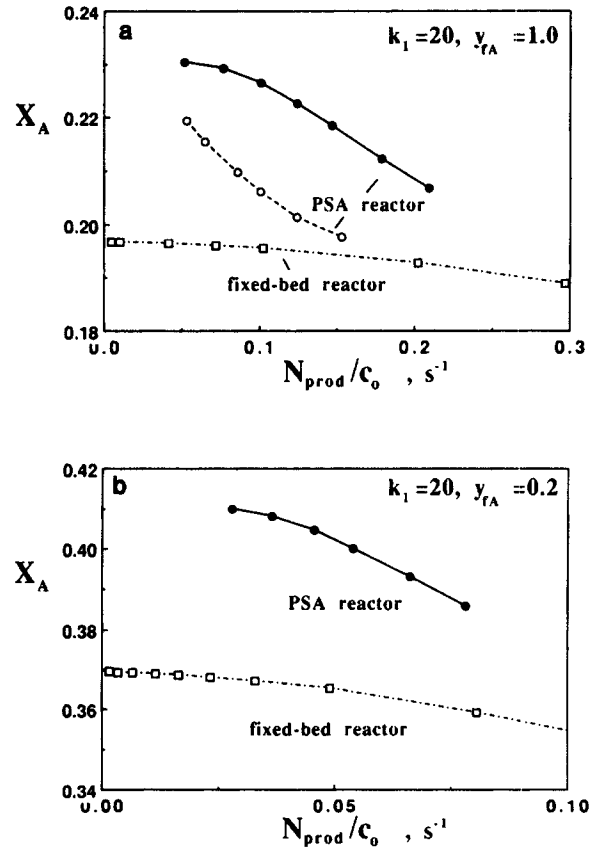

Figure 8. Conversion of the reactant A as a function of the productivity of the catalyst/adsorbent obtained from the PSA reactor and fixed-bed reactor: $b_A = 0$ for full lines and $b_A = 20$ L/mol for dashed lines.

(a) For pure reactant A feed $y_{fA} = 1.0$; (b) For impure reactant A feed $y_{fA} = 0.2$.

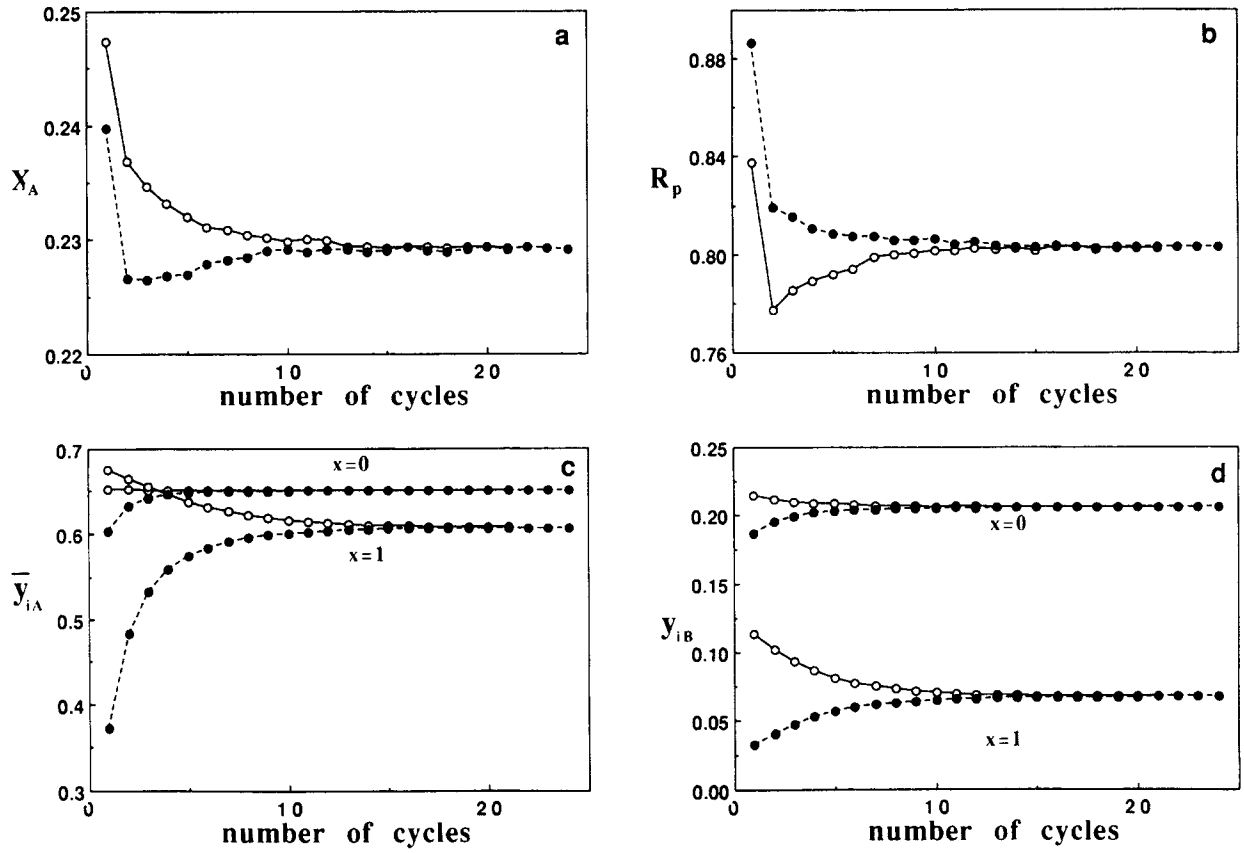

Figure 9. Evolution of the process parameters.

(a) Conversion of the reactant X_A; (b) production ratio R_p; (c) average mole fraction of the species $A\bar{y}_{iA}$ ($i=f, p$) in the product streams; (d) average mole fraction of the species $B\bar{y}_{iB}$ ($i=f, p$) in the product streams, from different initial conditions stated by Eq. 5 (dashed lines) and by Eq. 6 (full lines) for pure reactant feed $y_{fA}=1.0$.

From Figures 6 and 7, we can see that impure reactant feed $y_{fA}<1$ to the PSA reactor process results in a lower enhanced conversion over the reaction equilibrium limit X_A/X_o and it decreases when the feed composition of the reactant y_{fA} decreases. For a given adsorbent capacity, the effects of the kinetic constant k_1 and the production ratio R_p on the enhanced conversion are less significant for lower feed composition of the reactant y_{fA}. The values used in Figure 7 were $q_m=0.5$ mol/L, $k_1=20$ s^{-1}, and $X_o=0.2597$ for $y_{fA}=0.5$.

Finally, the conversion as a function of the productivity of the catalyst/adsorbent N_{prod}/c_o from a PSA reactor process and a fixed-bed reactor at steady state is shown in Figure 8 for the case where only the product B is adsorbable (full lines). In this simulation $q_m=0.5$ mol/L, $\theta_i=11$, feed and purge rates vary with the productivity, and the ratio between purge and feed amounts $u_p^* f_t \theta_p / u_f^* f_h \theta_f$ is kept at 8/9 which leads to $R_p=0.81$ for $y_{fA}=1.0$ and $R_p=0.84$ for $y_{fA}=0.2$. From these results, it can be concluded that 10–20% higher conversion can be obtained from a three-step, one-bed PSA reactor than from a fixed-bed reactor with comparable productivity. The enhancement of the conversion in the PSA reactor is mainly dependent on the adsorption isotherm of the adsorbable species, feed composition of the reactant, and operating conditions of the PSA reactor.

Evolution of the PSA Reactor Process from Different Initial Conditions and the Bed Dynamics of the Process at the Cyclic Steady State. The simulations of evolution of a three-step (pressurization, feed, and blowdown), one-column PSA process from different initial conditions has been studied by Lu et al. (1993b). No multiple steady states were found. In this three-step (feed, delay, and purge), one-bed PSA reactor, the process parameters: conversion X_A, production ratio R_p, and average mole fractions of species A, B, and C in the two streams obtained at two ends of the reactor, as a function of the number of the cycles for different initial conditions $y_{Ao}=0$, $y_{Bo}=0$, and $y_{Co}=1$ for $y_{fA}=1$ and $y_{Co}=0$ for $y_{fA}=0.2$ (Eq. 5, dashed lines) and $y_o=0.2$ for $y_{fA}=1$ and $y_o=0.074$ for $y_{fA}=0.2$ (Eq. 6, full lines) are shown in Figures 9 and 10 for $y_{fA}=1$ and $y_{fA}=0.2$, respectively, where $q_m=0.5$ mol/L and $k_1=20$ s^{-1}. Each process parameter in these figures for different initial conditions goes to the same value at the cyclic steady state. This behavior has been checked for various operating conditions. At the cyclic steady state the axial mole fraction profiles are exactly recovered whatever initial condition is used. Normally, the number of cycles needed for the process to reach the cyclic steady state is around 20–40 cycles, and it increases with the adsorption capacity q_m. Also, the process with impure reactant feed needs more cycles to reach the cyclic steady state than that with pure reactant feed for similar operation conditions.

The bed dynamics is very important to understand the process operation and to find better operating conditions to improve the process performance. In this section, we will mainly focus on the bed dynamics of individual steps of the process

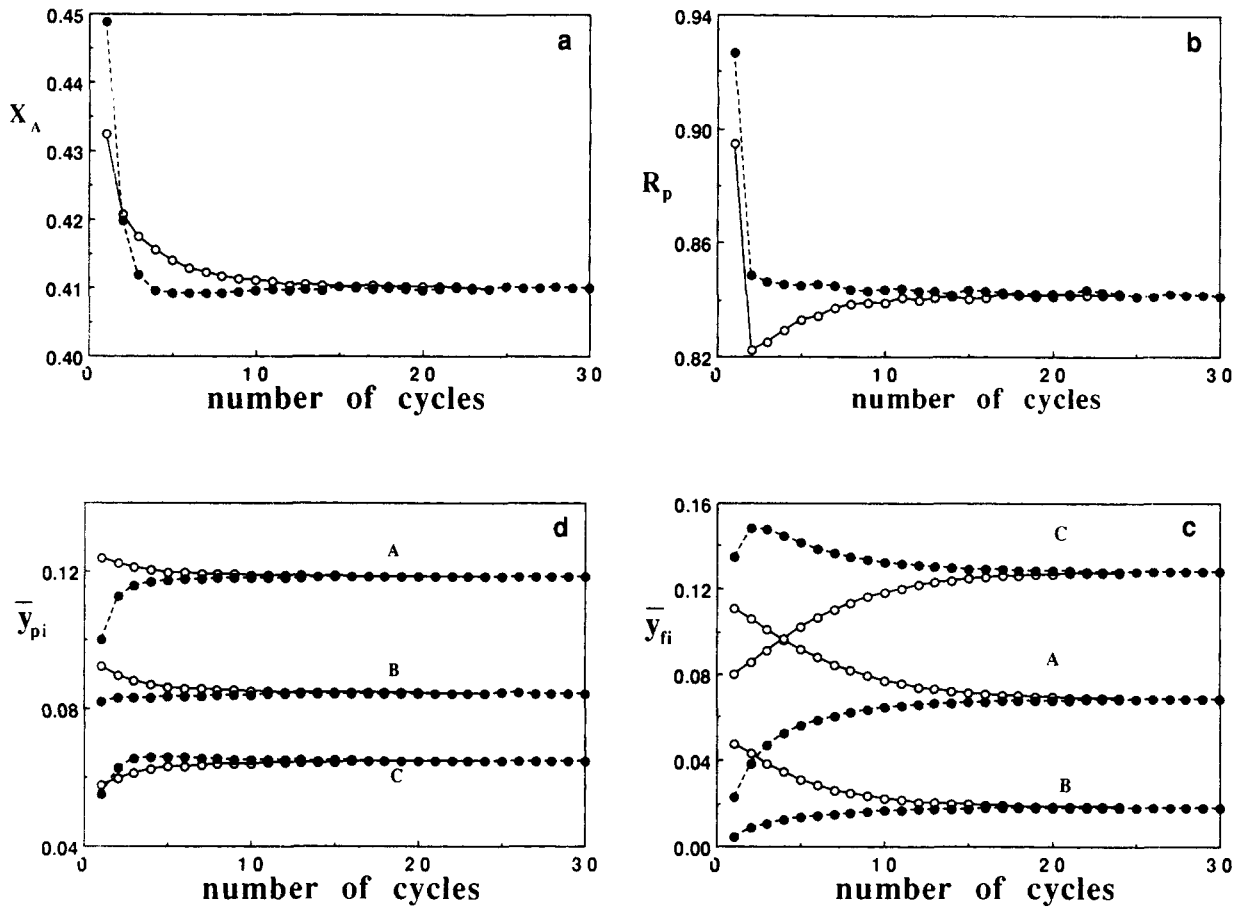

Figure 10. Evolution of the process parameters.

(a) Conversion of the reactant X_A; (b) production ratio R_p; (c) average mole fraction of the species in the product stream obtained at $x=1$ $\bar{y}_{fi}$ ($i=A$, B, C); (d) average mole fraction of the species in the product stream obtained at $x=0$ $\bar{y}_{pi}$ ($i=A$, B, C), from different initial conditions stated by Eq. 5 (dashed lines) and by Eq. 6 (full lines) for impure reactant feed $y_{fA}=0.2$.

at the cyclic steady state. The simulation values used are the same as those listed in the paragraph above for $y_{fA}=1$.

(*a*) *Feed Step.* The axial profiles of reduced pressure f, reduced velocity u^*, mole fractions of species A and B y_A, y_B, and dimensionless concentration of species A and B fy_A, fy_B at different times in the feed step are shown in Figures 11a–11f, respectively. At relatively long times, very high pressure can be observed at the feed end of the bed due to high feed rate used. The fluid velocity at the open end of the bed is very high since the pressure at this end of the bed is kept at 1 bar and the mole flux u^*f increases along the bed because the reaction proceeds with increase in the number of moles. At short times, zero flow points can be found inside the bed because the pressure drop across the bed changes direction from the last step (purge step) to feed step.

Very large mole fraction gradients of the species A and B were observed at the feed end of the bed since reaction occurs inside the bed which leads to a difference between feed mole fraction and the mole fraction at $x=0$. A mass balance error was found in simulations if Danckwerts's boundary conditions were not used (Eq. 7) and it increases with the kinetic constant k_1 and decreases when the feed rate $u_f^* f_h$ decreases. After the large gradients of the mole fraction of the species A and B near $x=0$, mole fraction fronts of the species A are formed and they become more dispersive with time (Figure 11c); two extreme values (maximum and minimum values except the point $x=0$) in the axial profiles of the product B for relative long times can be observed (Figure 11d).

The dimensionless concentration of the species A inside the bed increases with time except near the open end of the bed; the axial profile smoothly decreases along the bed (Figure 11e). The concentration fronts of the species B can be seen in this step since B is adsorbable. The higher concentration peak increases with time; however, the lower concentration plateau at the downstream stays almost constant (Figure 11f).

(*b*) *Delay Step.* A delay used after feed is important to obtain high conversion. In this step, the feed end of the bed is closed; the other end of the bed is kept opened. Light species moves fast and so more of it goes out of the bed; the adsorbable species moves at slower velocities, then more amount remains in the bed. The pressure inside the bed decreases and the fluid velocity becomes smaller with time as shown in Figures 12a and 12b.

The mole fraction of the species A decreases largely at the closed end of the bed, and it increases slightly at the other end of the bed due to the pressure decrease inside the bed which is favorable to the reaction equilibrium. At relative long times, two mole fraction plateaus (peaks) can be seen in the axial

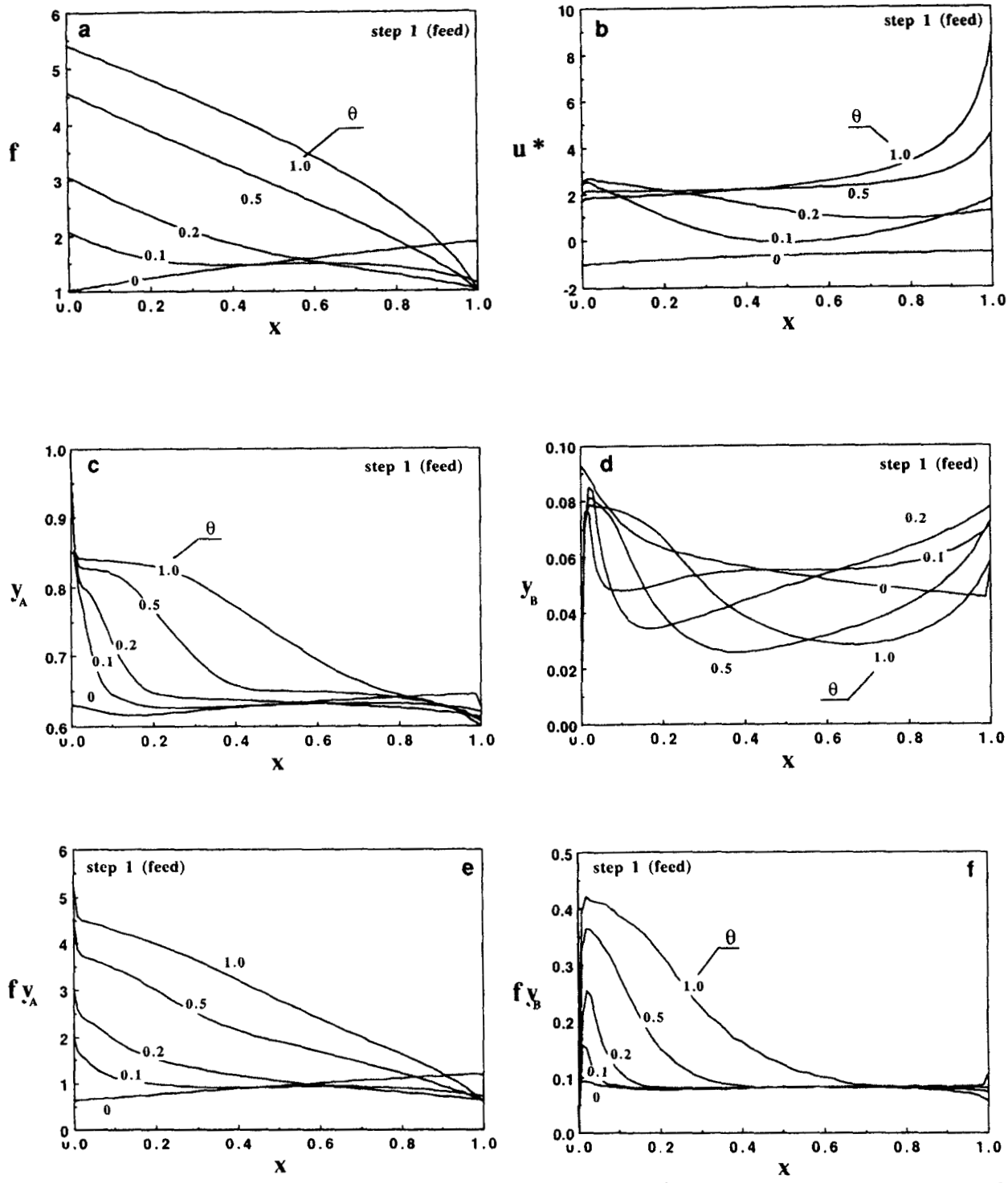

Figure 11. Axial profiles of the reduced pressure f (a); reduced velocity u^* (b); mole fractions of the species A, y_A (c); and B, y_B (d); dimensionless concentrations of the species A, fy_A (e); and B, fy_B (f) at different times during the feed step under the cyclic steady state for $y_{fA}=1.0$ and $b_A=0$.

profiles of the reactant A (Figure 12c). The mole fraction of the product B always increases inside the bed with time due to reactant conversion and desorption of the species retained in the solid phase when pressure decreases. This increase is more significant near the closed end of the bed, and finally the lower concentration plateau in the axial profiles formed in the last step disappears at relatively long times (Figure 12d).

No plateau is observed in the axial concentration profiles of the species A; the concentration decreases with time except at the open end of the bed where it is constant (Figure 12e).

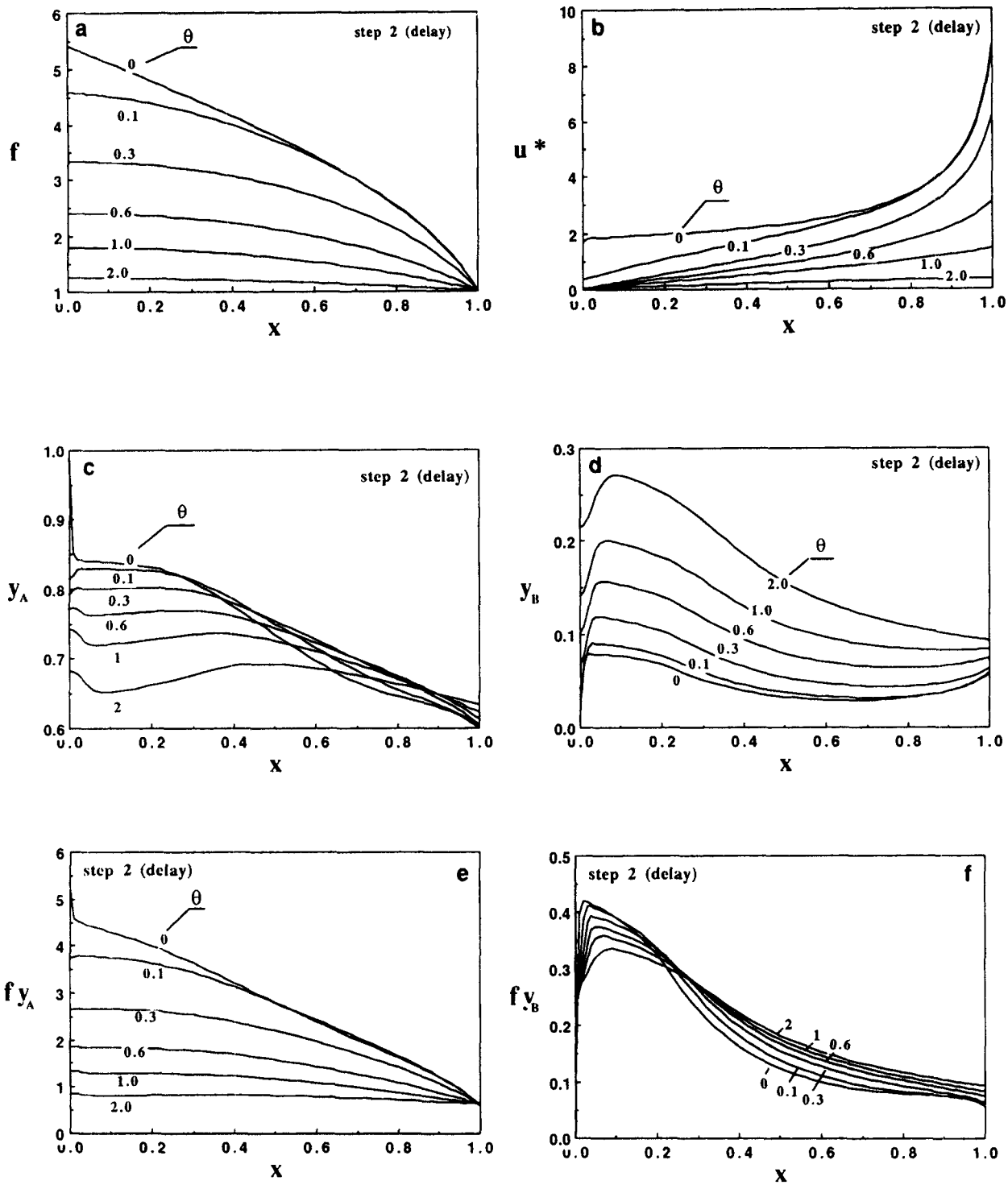

Figure 12. Axial profiles of the reduced pressure f (a); reduced velocity u^* (b); mole fractions of the species A, y_A (c); and B, y_B (d); dimensionless concentrations of the species A, fy_A (e); and B, fy_B (f) at different times during the delay step under the cyclic steady state for $y_{fA}=1.0$ and $b_A=0$.

At long times, the axial profile of the concentration is almost flat. The behavior of the axial profiles of the species B is somewhat different from that of its mole fraction. The concentration decreases near the closed end of the bed since there the pressure decrease dominates; and it increases at the other end of the bed since it moves with bulk fluid flow (Figures 12f).

(*c*) *Purge Step.* The behavior of axial profiles of reduced pressure and reduced velocity in the purge step, shown in Figures 13a and 13b, are similar to those observed in the feed

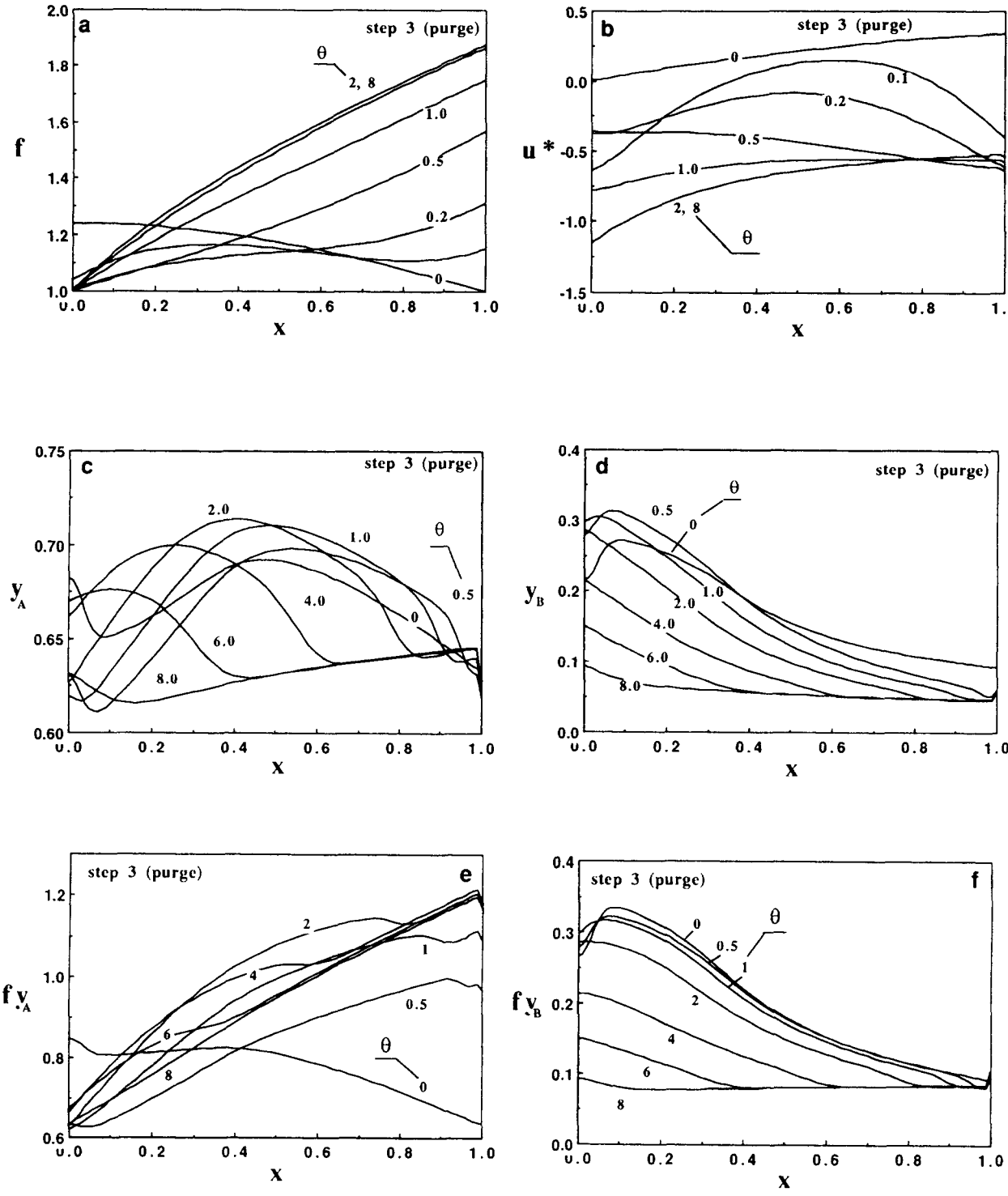

Figure 13. Axial profiles of the reduced pressure f (a); reduced velocity u^* (b); mole fractions of the species A, y_A (c); and B, y_B (d); dimensionless concentrations of the species A, fy_A (e); and B, fy_B (f) at different times during the purge step under the cyclic steady state for $y_{fA} = 1.0$ and $b_A = 0$.

step; only their values are relatively smaller and their position is reversed. At long times, these profiles almost do not change. In Figures 13c and 13d, relative high mole fraction gradients of the species A and B can also be seen at the purge end of the bed since the purge stream used is the product obtained in the feed and delay steps. The mole fraction profiles of species A and B move out of the bed at the open end with time (Figures 13c and 13d); however, the waves in the axial profiles of the species A almost disappear (Figure 13e).

Now, we can easily understand the results obtained in Figure 4. If the purge time is higher, that is, more purge amount which means higher production ratio R_p, the mole fraction or

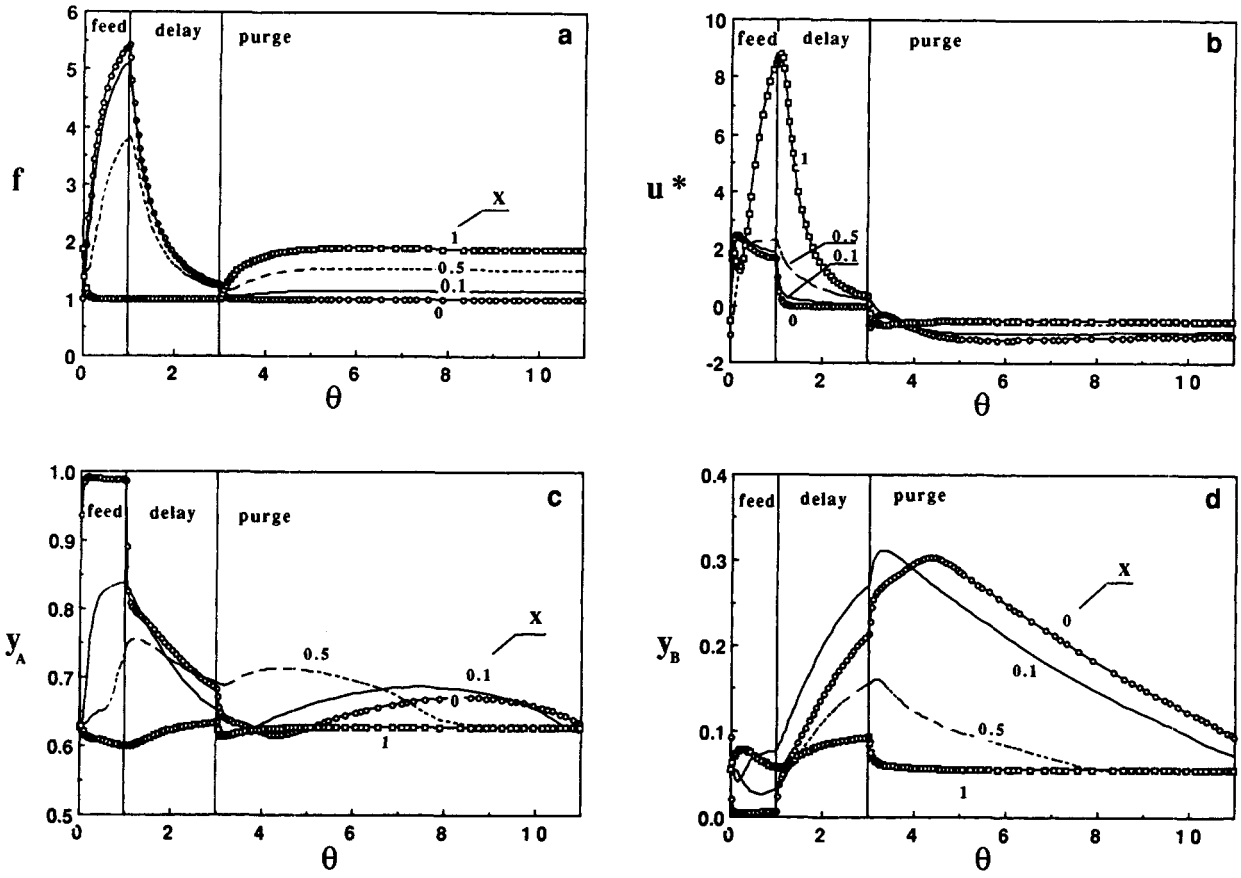

Figure 14. Histories of the reduced pressure f (a); reduced velocity u^* (b); mole fractions of the species A, y_A (c); and B, y_B (d) at different four spatial positions $x=0$, 0.1, 0.5, 1 during one complete cycle under the cyclic steady state for $y_{fA}=1.0$ and $b_A=0$.

the concentration of the species B at $x=0$ is almost kept constant since a plateau is reached (Figures 13d and 13f); however, the mole fraction of the species A, that is, the concentration of reactant A at the bed outlet, will increase with the purge amount after its minimum value moves out of the bed (Figure 13c). Before this minimum value in the axial profiles of the species A reaches $x=0$, the conversion increases with the production ratio R_p and after that the conversion decreases with R_p. This minimum value corresponds to the maximum point in the plot of X_A/X_o vs. R_p shown in Figure 4a.

For higher adsorption capacity of the catalyst-adsorbent, the penetration distance of the adsorbable species, that is, wave front of the adsorbable species, coinciding with reactant A is smaller in the feed step (Lu et al., 1993c), so it is near the feed end in the delay step. The mole fraction or concentration of species B observed in purge step (Figures 13d and 13f) will appear at $x=0$ earlier with increase of the purge time, that is, purge amount, and so the production ratio R_p, which results in that conversion X_A reaches its maximum value earlier with increase of the production ratio R_p. For smaller adsorption capacity, the penetration distance is larger and then the plateau will appear at $x=0$ later. Since the purge amount cannot be larger than the amount obtained in feed and delay steps, that is, R_p cannot be larger than unity, the plateau in the axial concentration profile of the species B in the purge step will never reach the outlet of the bed, so there is no maximum point in the X_A/X_o vs. R_p plot for low adsorption capacity.

Histories of reduced pressure f, reduced velocity u^*, and mole fractions of species A and B, y_A, y_B, at four spatial positions of the bed $x=0$, 0.1, 0.5, 1 in one cycle are shown in Figures 14a, b, c, d, respectively. The bed dynamics studied from the axial profiles for different times inside the bed can also be understood from these figures.

When the feed stream is a mixture of reactant A and inert I, the bed dynamics at the cyclic steady state is very similar to that with pure reactant feed. For comparison, histories of the several parameters at four bed position for $y_{fA}=0.2$ are shown in Figure 15. Other values used in the simulation are the same as those for $y_{fA}=1$.

Reactant A and product B both are adsorbed ($b_A \neq 0$)

In the last section, we discussed the system in which only the product B is adsorbable and found that the performance of a PSA reactor was better than that from a fixed-bed reactor. As a starting point, it is convenient to assume that the reactant species A is nonadsorbable; however, this assumption is not true for many dehydrogenation catalytic reactions (Schweich and Villermaux, 1982; Antonucci et al., 1978). In the following part of this work, the system in which the reactant A and one product B are both adsorbable and B is more adsorbable than A (Schweich and Villermaux, 1982; Antonucci et al., 1978) is considered.

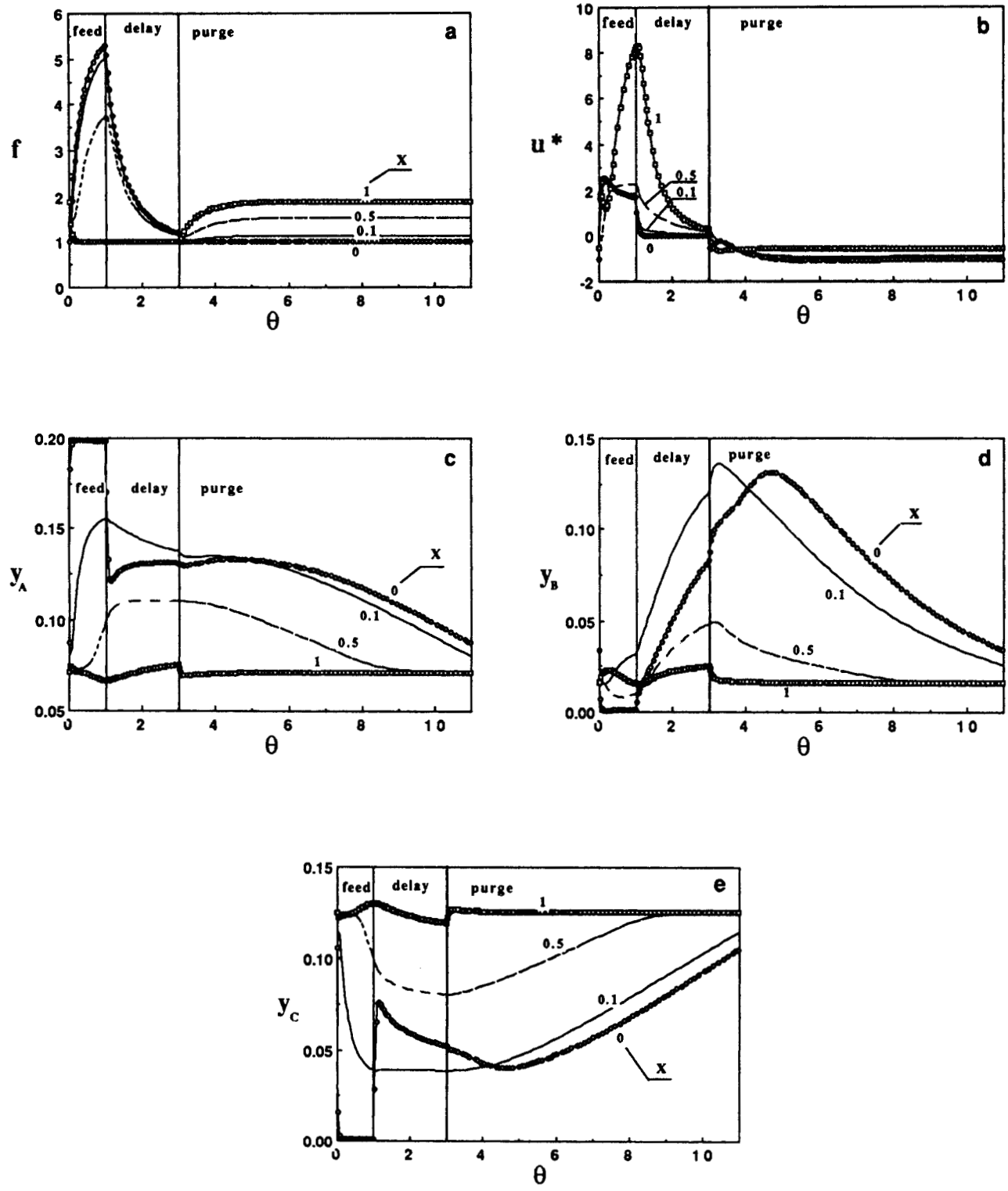

Figure 15. Histories of the reduced pressure f (a); reduced velocity u^* (b); mole fractions of the species A y_A (c); and B y_B (d); and C y_C (e) at different four spatial positions $x = 0$, 0.1, 0.5, 1 during one complete cycle under the cyclic steady state for $y_{fA} = 0.2$ and $b_A = 0$.

Process Performance of the PSA Reactors: (*a*) *Pure Reactant A feed, $y_{fA} = 1$.* When the reactant A is adsorbable on the catalyst/adsorbent, the competitive multicomponent extended Langmuir isotherm was used in the simulations, with $b_B = 50$ L/mol. The enhanced conversion over the reaction equilibrium limit X_A/X_o and the separation factor α_{BA} as a function of the production ratio R_p for different adsorption affinity coefficient of the reactant A, $b_A = 0$, 10, 20 L/mol,

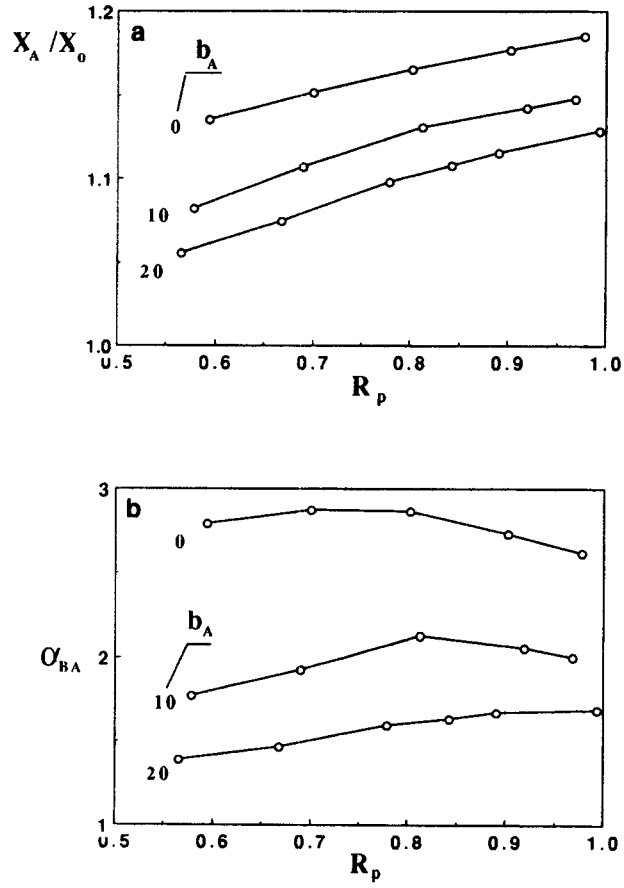

Figure 16. Enhanced conversion X_A/X_o (a); and separation factor α_{BA} (b) as a function of the production ratio R_p for different adsorption affinity coefficients of the reactant A $b_A = 0$, 10, 20 L/mol and pure reactant feed $y_{fA} = 1$.

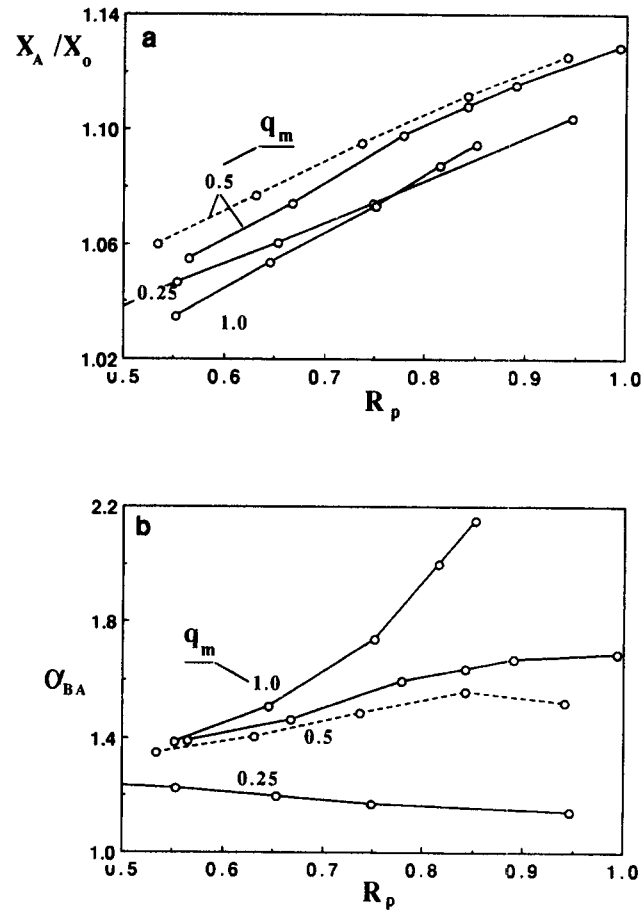

Figure 17. Enhanced conversion X_A/X_o (a); and separation factor α_{BA} (b) as a function of the production ratio R_p for different adsorption capacities $q_m = 0.25$, 0.5, 1.0 mol/L and pure reactant feed $y_{fA} = 1$.

are shown in Figures 16a and 16b, respectively, and the other values used were: $q_m = 0.5$ mol/L, $k_1 = 20$, $u_f^* f_h = 9$, $\theta_f = 1$, $\theta_d = 4$, $u_p^* f_f = 1$, and $\theta_p = 6$–11. The general behavior of the relationships of X_A/X_o vs. R_p and α_{BA} vs. R_p does not vary much for different values of b_A; however, the values of the conversion X_A and separation factor α_{BA}, that is, process performance, significantly decrease when b_A increases for given operating conditions. It was found that for the same value of production ratio R_p, the purge amount needed is larger for higher values of b_A. This can be understood since in this reversible reaction, the reactant A and product B are always present at the same time due to reaction equilibrium. The forward reaction rate is proportional to the reactant concentration in the fluid inside the pores of the catalyst/adsorbent; therefore, the reactant A adsorbed will be purged out of the bed after the delay step.

The effect of the adsorption capacity on the process performance is shown in Figure 17 in full lines where $b_A = 20$ L/mol and $k_1 = 20\ s^{-1}$. The conversion first increases and then decreases with increase of the adsorption capacity; there is an intermediate value of q_m which gives the highest conversion obtained for given operating conditions. This result is different from what was found for the system in which only B is adsorbed. Also the effect of feed rate on the conversion presented

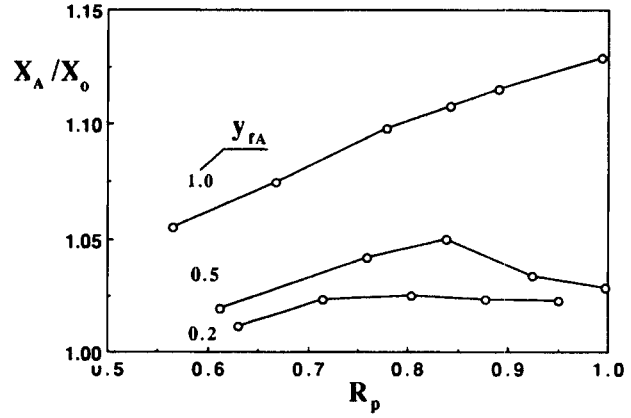

Figure 18. Enhanced conversion X_A/X_o as a function of the production ratio R_p for different feed compositions $y_{fA} = 0.2$, 0.5, 1.0 in the case where both the reactant A and product B are adsorbable.

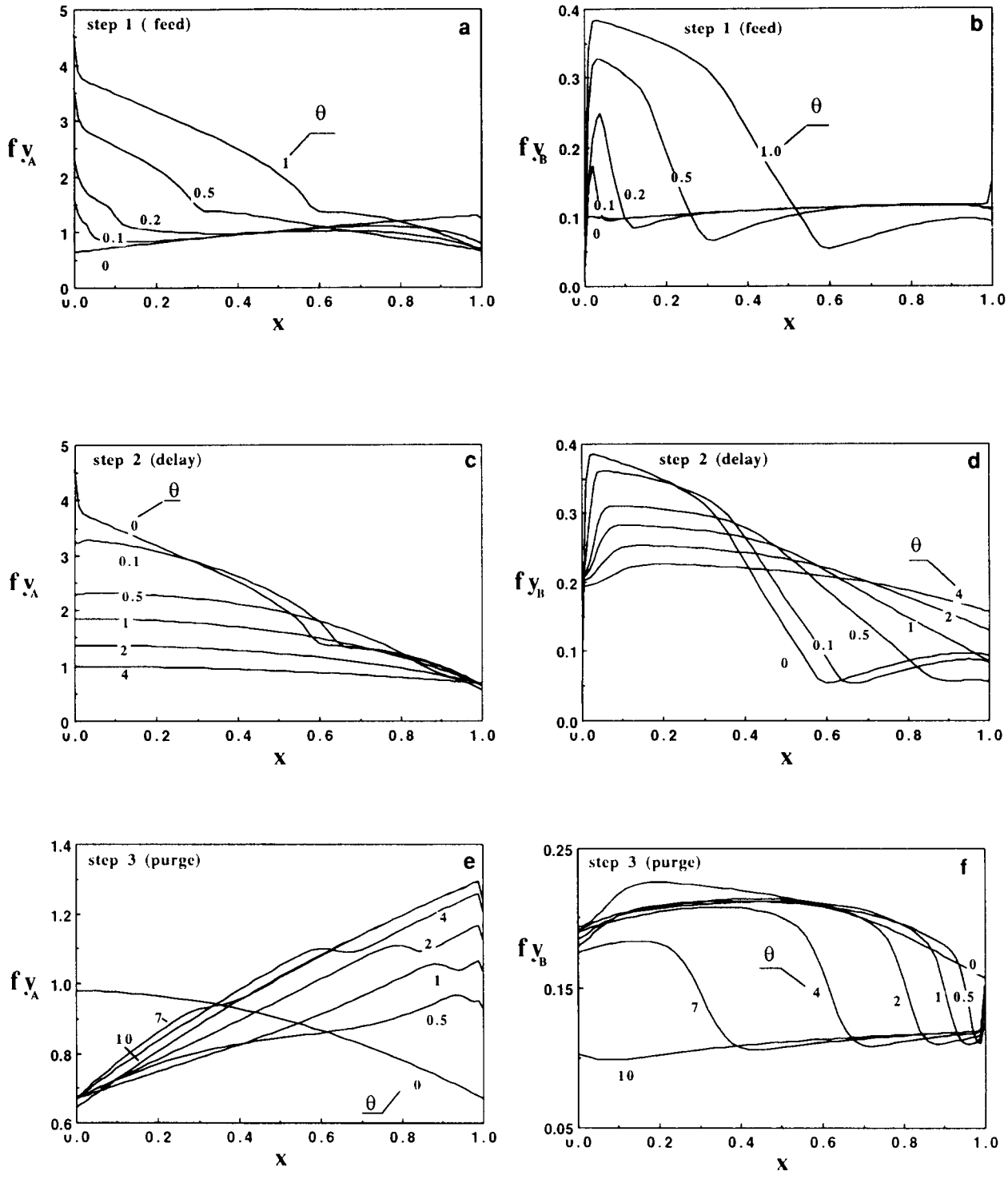

Figure 19. Axial profiles of the dimensionless concentration of the species *A* and *B* at different times during the feed step (a, b); delay step (c, d); and purge step (e, f), respectively, under the cyclic steady state for $y_{fA}=1.0$ and $b_A=20$ L/mol.

in Figure 17 (dashed lines for $u_f^* f_h=4.5$, $\theta_f=2$) is opposite to the one found above.

The effect of the kinetic constant k_1 on the process parameters for the case where $q_m=0.5$ mol/L, $b_A=20$ L/mol, and $R_p=0.89$ is shown in Figure 6 (dashed lines). The behavior is similar to that for $b_A=0$, but leads to smaller values of the performance parameters. The conversion as a function of the productivity of the catalyst/adsorbent is presented in Figure 8a in dashed line with the same values used before where $u_p^* f_t \theta_p / u_f^* f_h \theta_f$ is kept at 10/9.

Process Performance of the PSA Reactors: (b) Effect of the Reactant Composition in the Feed, y_{fA}. When the feed

stream is not the pure reactant A, the enhanced conversion over the reaction equilibrium limit from the PSA reactor largely decreases when y_{fA} decreases as shown in Figure 18, where $q_m = 0.5$ mol/L, $b_A = 20$ L/mol, and $k_1 = 20\ s^{-1}$. The conversion is only 2.5% higher than reaction equilibrium conversion for $y_{fA} = 0.2$ in this PSA reactor process. This is because the feed components A and I are separated in the bed since A is adsorbable; as a result more concentrated reactant A is obtained near the feed end of the bed and so lower conversion is in that region as compared to the one observed in the fixed-bed reactor operation. This three-step, one-column PSA reactor is obviously not suitable for this reaction system to obtain high conversion, therefore some other operating schemes must be explored as discussed later.

Bed Dynamics of the PSA Reactor at the Cyclic Steady State for $y_{fA} = 1$. We briefly discuss the bed dynamics to understand the process behavior and then explore new operating schemes. The reference case is based on the following values: $q_m = 0.5$ mol/L, $b_A = 20$ L/mol, $k_1 = 20\ s^{-1}$, $u_f^* f_h = 9$, $\theta_f = 1$, $\theta_d = 4$, $u_p^* f_\ell = 1$, $\theta_p = 10$, and $R_p = 0.89$.

The evolution of the process from different initial conditions has also been studied, and various results were found for the same operating conditions. The number of cycles to reach the cyclic steady state is around 30–50 cycles which is larger than in the case where only B is adsorbable.

The behavior of pressure and velocity inside the bed in individual steps is very similar to that shown above; only the pressure at the feed end and the velocity at the open end of the bed in feed and delay steps are a little smaller since reactant A is adsorbed.

Very clear concentration wave fronts of the species B can be observed in the feed step as shown in Figure 19b. These concentration fronts become dispersive with time in the delay step, and at a relatively long time the axial profiles of the concentration of the species A and B almost reach flat lines as shown in Figures 19c and 19d. This behavior is very different from that observed in the case where the reactant is nonadsorbable. In the purge step, the concentration waves of the species B also move towards the open end of the bed with time; however, the amplitude of the waves is much smaller than those found in Figure 13.

New operating schemes for the PSA reactor processes

In the last work (Lu et al., 1993a), alternate layers of catalyst/adsorbent and adsorbent inside the bed were considered. Simulation showed a better process performance than that obtained when only catalyst/adsorbent was used for systems in which the reactant A and product B are both adsorbable and the purge is not introduced. However, this arrangement does not help much when the purge is used.

According to our understanding of the behavior of the PSA reactor process, the operating scheme of a three-step two-bed PSA reactor process, as shown in Figure 20, is explored in this work. The model equations in this process are the same as that for the three-step one-bed PSA reactor process derived above except the boundary conditions become:

Feed (Step 1) $(0 \le \theta \le \theta_f)$:

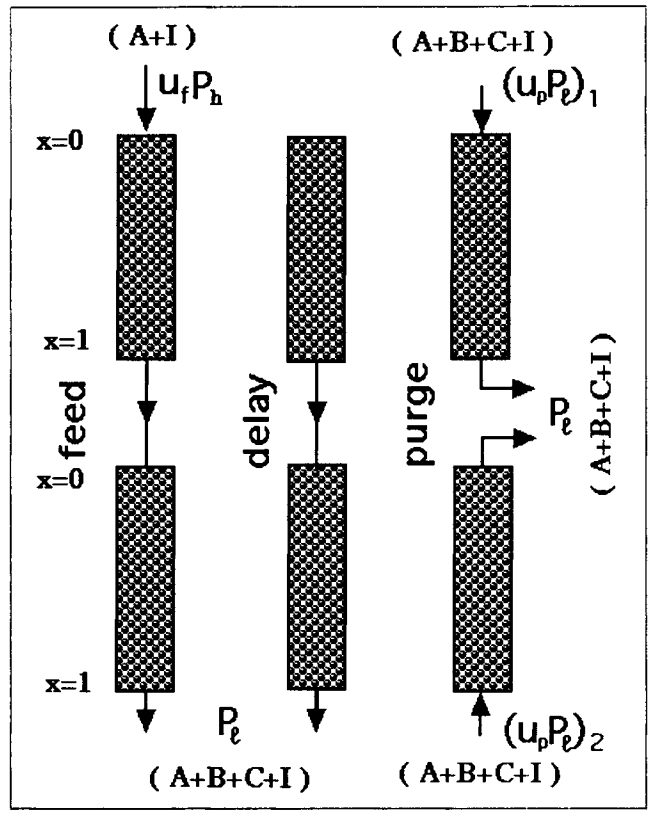

Figure 20. Operating scheme of the three-step, two-bed PSA reactors.

Bed 1

$$x=0,\quad u^* f = u_f^* f_h,\quad -\frac{1}{Pe}\frac{\partial y_A}{\partial x} + y_A = 1,$$

$$-\frac{1}{Pe}\frac{\partial y_i}{\partial x} + y_i = 0 \ (i = B, C) \qquad (23)$$

$$x=1,\quad f = (f|_{x=0})_{\text{bed2}},\quad \frac{\partial y_i}{\partial x} = 0 \ (i = A, B, C) \qquad (24)$$

Bed 2

$$x=0,\quad u^* f = [(u^* f)|_{x=1}]_{\text{bed1}},$$

$$-\frac{1}{Pe}\frac{\partial y_i}{\partial x} + y_i = (y_i|_{x=1})_{\text{bed1}} \ (i = B, C) \qquad (25)$$

$$x=1,\quad f = f_\ell,\quad \frac{\partial y_i}{\partial x} = 0 \ (i = A, B, C) \qquad (26)$$

Delay (Step 2) $(0 \le \theta \le \theta_d)$:

Bed 1

$$x=0,\quad \frac{\partial f}{\partial x} = 0,\quad \frac{\partial y_i}{\partial x} = 0 \ (i = A, B, C) \qquad (27)$$

$$x=1, \quad f=(f|_{x=0})_{\text{bed2}}, \quad \frac{\partial y_i}{\partial x}=0 \ (i=A, B, C) \qquad (28)$$

Bed 2

same as that stated in Eqs. 25 and 26

Purge (Step 3) $(0 \le \theta \le \theta_p)$:

Bed 1

$$x=0, \quad u^*f=(u_p^*f_\theta)_{\text{bed1}}, \quad -\frac{1}{Pe}\frac{\partial y_i}{\partial x}+y_i=\bar{y}_{fi} (i=A, B, C) \qquad (29)$$

$$x=1, \quad f=f_\ell, \quad \frac{\partial y_i}{\partial x}=0 \ (i=A, B, C) \qquad (30)$$

Bed 2

$$x=0, \quad f=f_\ell, \quad \frac{\partial y_i}{\partial x}=0 \ (i=A, B, C) \qquad (31)$$

$$x=1, \quad u^*f=-(u_p^*f_\theta)_{\text{bed2}}, \quad -\frac{1}{Pe}\frac{\partial y_i}{\partial x}+y_i=\bar{y}_{fi} \ (i=A, B, C) \qquad (32)$$

where $\bar{y}_{fi}$ is the average mole fraction of species i ($i = A, B, C$) in the stream obtained at the outlet of the bed 2 in the feed and delay steps.

Numerical simulations were carried out for the process described above. It is very time consuming to verify the boundary conditions between the two beds during the integrations since they vary with time; around 20 minutes are needed for simulating a cycle in the computer.

Here, we present simulation results of one run where: $q_m=0.5$ mol/L, $b_A=20$ L/mol, $b_B=50$ L/mol, $k_1=20$ s^{-1}, $y_{fA}=0.2$, $u_f^*f_h=9$, $\theta_f=3$, $\theta_d=5$, $(u_p^*f_\theta)_{\text{bed1}}=1$, $(u_p^*f_\theta)_{\text{bed2}}=0.1$, and $\theta_p=15$. Under these conditions we got $X_A/X_o=110\%$, $R_p=0.94$ (product obtained in the purge step over that obtained in a complete cycle), $\alpha_{BA}=1.5$, $\alpha_{BA}=3.95$ (the selectivity of the species in the product stream obtained in the feed/delay and purge steps in a complete cycle), and $N_{\text{prod}}/c_o=0.021$ s^{-1}. Under the cyclic steady state, high concentration of the reactant A and product B was observed in the feed and delay steps inside bed 1; they were very low inside bed 2, and both the average mole fractions of the species A and B obtained in the feed and delay steps are less than 1%. A more careful selection of the operating conditions may give better reaction performance of the process. It is expected that this operating scheme will be suitable for systems where both the reactant A and product B are adsorbable and A is even more adsorbable than B.

Conclusions

A mathematical model for the pressure swing adsorption reactor has been proposed in this article and used to analyze the reaction performance in a three-step (feed, delay, and purge) one-bed operating scheme. The model consists of species and overall mass balances, momentum balance, reaction rate, and multicomponent adsorption equilibrium isotherms. Three main problems were studied: reaction performance of the PSA reactor process under various system and operating parameters, evolution of the process from different initial conditions, and bed dynamics at the cyclic steady state.

In the parametric studies, we considered the effect of adsorption affinity coefficient of the reactant species, adsorption maximum capacity, feed composition, reaction rate, feed and purge rates, and delay time. When the reactant is not adsorbable, conversion of the reactant from the PSA reactor 10–20% higher than that from the fixed-bed reactor with comparable productivity of the catalyst/adsorbent was obtained under various conditions. Higher maximum adsorption capacity, higher reaction kinetic constant, and higher feed rate give higher conversion of the reactant; lower feed composition of the reactant leads to lower enhanced conversion over the reaction equilibrium limit value. For relative low adsorption capacity, larger purge amount results in better reaction performance; however, there is a optimum purge amount for relative high adsorption capacity. When the reactant is adsorbable, the conversion largely decreases with the increase of the adsorption affinity coefficient of the reactant; however, 10% higher conversion over the reaction equilibrium limit value was still observed for pure reactant feed. This three-step, one-bed PSA reactor operating scheme does not seems suitable if the feed is not pure reactant.

The evolution of the PSA reactor process from different initial conditions to the cyclic steady state was addressed by looking at the changes of process parameters; no multiple cyclic steady states were found. The number of the cycles to reach the cyclic steady state increases with increase of adsorption capacity and adsorption affinity coefficient of the reactant and decrease of the feed composition of the reactant. The bed dynamics have been studied in the three individual steps (feed, delay, and purge). From the development of the axial profiles of the variables inside the reactor, we understood and explained the results found for the global process performance; they also provide clues to explore new operating schemes of the PSA reactors.

Finally, a three-step (feed, delay, and purge), two-bed pressure swing reactors operating scheme was explored; simulation results showed that in this process one could obtain more than 10% higher conversion of the reactant over the reaction equilibrium limit value for the case where the reactant is adsorbable and the feed is impure reactant.

Notation

b_i = extended multicomponent Langmuir isotherm parameters ($i=A, B$), m^3/mol
$b_1, \ldots, b_4$ = dimensionless constants
c = total concentration in the bulk fluid phase, mol/m^3
c_o = total concentration in the bulk fluid phase under reference conditions, mol/m^3
d_p = adsorbent particle diameter, m
D = bed diameter, m
D_{ax} = axial mass dispersion coefficient, m^2/s
D_{mo} = molecular diffusivity at reference conditions, m^2/s
f = dimensionless total concentration in the bulk fluid phase
f_h = dimensionless high pressure
f_ℓ = dimensionless low pressure
k_1 = forward reaction kinetic coefficient, s^{-1}
k_2 = backward reaction kinetic coefficient, m^3/mol·s

K_e = reaction equilibrium constant, m^3/mol
K_T = dimensionless reaction equilibrium constant
L = bed length, m
N_b = dimensionless output rate at the feed end of the bed in a cycle
N_i = dimensionless output rate of the species i ($i=A, B, C$) (Eq. 19)
N_t = dimensionless total output rate of the bed in a cycle
N_{prod} = productivity of the unit catalyst (Eq. 20), $mol/m^3 \cdot s$
P = pressure in the bulk fluid, Pa
P_h = high pressure, Pa
P_l = low pressure, Pa
P_o = atmospheric pressure or reference pressure, Pa
Pe = Peclet number in the bulk fluid, dimensionless
q_m = maximum adsorption capacity in Langmuir isotherm, mol/m^3
R_p = production ratio
t = time, s
T = temperature, K
To = reference temperature, K
u = superficial velocity in the bulk fluid, m/s
u_o = superficial velocity under the reference conditions, m/s
u^* = dimensionless velocity in the bulk fluid
u_f^* = dimensionless feed velocity
u_p^* = dimensionless purge velocity
x = dimensionless axial coordinate in the bed
X_A = reaction conversion
y_i = mole fraction of species in the bed ($i=A, B, C$)
$\bar{y}_{fi}$ = average mole fraction of species at $x=1$ ($i=A, B, C$)
$\bar{y}_{pi}$ = average mole fraction of species at $x=0$ ($i=A, B, C$)

Greek letters

α_{Bi} = separation factor ($i=A, C$) (Eq. 21)
γ_1, γ_2 = parameters
ϵ = bed porosity
ϵ_p = adsorbent porosity
θ = time reduced by the reference space time
$\theta_t, \theta_f, \theta_p, \theta_b$ = dimensionless cycle, feed, production, and blowdown times, respectively
μ = fluid viscosity, kg/ms
ρ_o = fluid density, kg/m^3

Literature Cited

Antonucci, P., N. Giordano, and C. J. Bart, "Chemical Reactions in Chromatographic Columns: Dehydrogenation of Ethane over Cadmium-Exchanged Zeolite 4Å," *J. Chromat.*, **150**, 309 (1978).

Carr, R. W., "Continuous Reaction Chromatography," in *Preparative and Production Scale Chromatography*, G. Ganetsos and P. E. Barker, eds., Marcel Dekker, New York, pp. 421-447 (1993).

Carta, G., "Simultaneous Reaction and Chromatography," in *Chromatography and Membrane Processes in Biotechnology*, C. Costa and J. Cabral, eds., Kluwer Acad. Publications, Dordrecht (1991).

Chatsiriwech, D., E. Alpay, L. S. Kershenbaum, and N. F. Kirkby, "The Enhancement of Catalytic Reaction by Pressure Swing Adsorption," published in *Proceedings of CHEMPOR'93, International Chem. Eng. Conf.*, Porto, Portugal (Apr. 4-6, 1993).

Coca, J., G. Adrio, C. Y. Jeng, and S. H. Langer, "Gas and Liquid Chromatographic Reactors," in *Preparative and Production Scale Chromatography*, G. Ganetsos and P. E. Barker, eds., Marcel Dekker, New York, pp. 449-475 (1993).

Fish, B. B., and R. W. Carr, "An Experimental Study of the Countercurrent Moving-Bed Chromatographic Reactor," *Chem. Eng. Sci.*, **44**, 1773 (1989).

Frey, D. D., and A. E. Rodrigues, "Explicit Calculation of Multicomponent Equilibria for Ideal Adsorbed Solutions," *AIChE J.*, **40**(1), 182, (1994).

Ganetsos, G., P. E. Barker, and J. N. Ajongwen, "Batch and Continuous Chromatographic Systems as Combined Bioreactor-Separators," in *Preparative and Production Scale Chromatography*, G. Ganetsos and P. E. Barker, eds., Marcel Dekker, p. 375 (1993).

Hashimoto, K., S. Adachi, and Y. Shirai, "Development of New Bioreactors of a Simulated Moving-Bed Type," in *Preparative and Production Scale Chromatography*, G. Ganetsos and P. E. Barker, eds., Marcel Dekker, pp. 395-419 (1993).

Loureiro, J. M., R. C. Soares, and A. E. Rodrigues, "Dynamics of Adsorptive Reactors," in *Preparative and Production Scale Chromatography*, G. Ganetsos and P. E. Barker, eds., Marcel Dekker, pp. 742-767 (1993).

Lu, Z. P., J. M. Loureiro, and A. E. Rodrigues, "Simulation of Pressure Swing Adsorption Reactors," published in *Proceedings of CHEMPOR'93, International Chem. Eng. Conf.*, Porto, Portugal (Apr. 4-6, 1993a).

Lu, Z. P., J. M. Loureiro, M. D. LeVan, and A. E. Rodrigues, "Simulation of a Three-Step One-Column Pressure Swing Adsorption Process," *AIChE J.*, **39**(9) p. 1483 (1993b).

Lu, Z. P., J. M. Loureiro, M. D. LeVan, and A. E. Rodrigues, "Pressurization and Blowdown of Adsorption Beds II: Effect of the Momemtum and Equilibrium Relations on Isothermal Operation," *Chem. Eng. Sci.*, **48**, 1699 (1993c).

Magee, E. M., "The Course of a Reaction in a Chromatographic Column," *Ind. Eng. Chem. Fundam.*, **2**, 32 (1963).

Madsen, N. K., and R. F. Sincovec, "PDECOL: General Collocation Software for Partial Differential Equations," *ACM Trans. Math. Software*, **5**(3), 326 (1979).

Matsen, J. M., J. W. Harding, and E. M. Magee, "Chemical Reaction in Chromagraphic Column," *J. Phys. Chem*, **69**(2), 522 (1965).

Petroulas, T., R. Aris, and R. W. Carr, "Analysis and Performance of a Countercurrent Moving-Bed Chromatographic Reactor," *Chem. Eng. Sci.*, **40**, 2233 (1985).

Roginskii, S. Z., M. I. Yanovskii, and G. A. Gaziev, "Chemical Reaction under Chromatographic Conditions," *Dokl. Akad. Nauk. USSR*, English Translation 041109500, **140**, 771 (1961).

Sardin, M., D. Schweich, and J. Villermaux, "Preparative Fixed-Bed Chromatographic Reactor," in *Preparative and Production Scale Chromatography*, G. Ganetsos and P. E. Barker, eds., Marcel Dekker, pp. 477-521 (1993).

Schweich, D., and J. Villermaux, "The Preparative Chromatographic Reactor Revisted," *Chem. Eng. J.*, **24**, 99 (1982b).

Schweich, D., and J. Villermaux, "Model for Catalytic Dehydrogenation of Cyclohexane in a Chromatographic Reactor: Comparison of Theory and Experience," *Ind. Eng. Chem. Fundam.*, **21**, 47 (1982a).

Skarstrom, C. W., U.S. Patent, 2,944,627 (1960).

van der Wielen, L., A. Straathof, and K. M. Luyben, "Adsorption and Chromatographic Bioreactors," in *Precision Process Technology*, M. Weijnen and A. Drinkenburg, eds., Kluwer Acad. Publications, Dordrecht (1993).

Vaporciyan, G. G., and R. H. Kadlec, "Equilibrium-Limited Periodic Separating Reactors," *AIChE J.*, **33**(8), 1334-1343 (Aug. 1987).

Vaporciyan, G. G., and R. H. Kadlec, "Periodic Separating Reactors: Experiments and Theory," *AIChE J.*, **35**(5), 831 (May 1989).

Viswanathan, S., and R. Aris, "Countercurrent Moving Bed Chromatographic Reactors," in *Chemical Reaction Engineering—II*, H. M. Hulburt, ed., Amer. Chem. Soc., Washington, DC (1974).

Wetherold, R. G., E. H. Wissler, and E. B. Bischoff, "An Experimental and Computational Study of the Hydrolysis of Methyl Format in a Chromatographic Reactor," in *Chemical Reaction Engineering—II*, H. M. Hulburt, ed., American Chemical Society, (1974).

Yang, R. T., *Gas Separation by Adsorption Processes*, Butterworths, Boston (1987).

Manuscript received July 1, 1993, and revision received Oct. 25, 1993.